Available online at www.sciencedirect.com

ScienceDirect

Geochimica et Cosmochimica Acta 170 (2015) 247–265

Geochimica et Cosmochimica Acta

www.elsevier.com/locate/gca

GEMS-like material in the matrix of the Paris meteorite and the early stages of alteration of CM chondrites

H. Leroux [a,*], P. Cuvillier [a], B. Zanda [b], R.H. Hewins [b]

[a] Unité Matériaux et Transformations, Université Lille 1 & CNRS, 59655 Villeneuve d'Ascq, France

[b] Institut de Minéralogie, de Physique des Matériaux, et de Cosmochimie (IMPMC), Sorbonne Universités, Muséum National d'Histoire Naturelle, UPMC Université Paris 06, UMR CNRS 7590, IRD UMR 206, 57 rue Cuvier, 75231 Paris, France

Received 26 July 2015; accepted in revised form 17 September 2015; Available online 28 September 2015

Abstract

The Paris meteorite is a weakly altered CM chondrite that has been discovered recently (Hewins et al., 2014). Its matrix offers the opportunity to search for well-preserved pristine pre-accretional material, as well as to study the earliest stages of aqueous alteration in the CM parent body. The study of the matrix of Paris has been conducted by analytical transmission electron microscopy on focused ion beam sections extracted from matrix areas showing different degrees of aqueous alteration.

The least altered matrix sample consists of amorphous silicate grains, a few hundreds of nm in size, separated from one another by an abundant porosity. The amorphous silicates enclose numerous Fe-sulfide nanograins and their average composition is close to the chondritic composition. They share many similarities with GEMS (glass with embedded metal and sulfides) grains present in chondritic-porous interplanetary dust particles and with primitive type 3.0 carbonaceous chondrites. This first discovery of GEMS-like texture in a CM chondrite suggests that GEMS grains could have been the building blocks of the CM matrices.

In more aqueously altered samples, pronounced microstructural heterogeneities were detected at the micrometer scale. The matrix consists mostly of a mixture of amorphous material and Fe-rich, spongy to fine-fibrous, poorly crystalline phyllosilicates. The porosity fraction is significantly reduced and the mixed amorphous-fibrous material frequently forms a continuous groundmass. The close association between these two material types suggests a replacement mechanism due to aqueous alteration. Chemical compositions correlate strongly with the microstructure. The amorphous material has a composition close to the chondritic value while the fine-fibrous phyllosilicate material is Fe-enriched. This Fe enrichment is found to be continuous from weakly to more heavily altered areas, in which the fibrous morphology is coarser and better crystalline. Cronstedtite with intercalated tochilinite is also found, but in pore spaces. This chemical evolution, concomitant with the maturation of the phyllosilicates, demonstrates that the early aqueous fluids that interacted with silicates in the matrix were enriched in Fe. This composition is probably the consequence of the preferential dissolution of metal and iron sulfides during the first stages of alteration. The enrichment of phyllosilicates in Mg seen in more altered CM chondrites is not observed in Paris.

1. INTRODUCTION

Carbonaceous chondrites are samples of parent bodies that are largely originated from the outer region of the asteroid belt. The most abundant of them are the CM chondrites. They all experienced an episode of aqueous and/or

* Corresponding author.
E-mail address: hugues.leroux@univ-lille1.fr (H. Leroux).

http://dx.doi.org/10.1016/j.gca.2015.09.019
0016-7037/

thermal alteration, to varied extents, likely in their parent bodies (e.g., McSween, 1979; Zolensky et al., 1993; Rubin et al., 2007; Alexander et al., 2013; Beck et al., 2014; Howard et al., 2015). The primary texture, mineralogy and/or isotopic properties are thus modified to some extent by the action of aqueous fluids (e.g., Brearley, 2006). The wide range of degree of alteration in CM chondrites provides the opportunity to study its different stages by tracking the associated mineralogical evolutionary sequences. Carbonaceous chondrites are characterized by a high proportion of matrix compared to chondrules, with an average of 70 vol.% for the CM chondrites. Matrices consist of fine-grained materials, most commonly sub-micrometer sized. As a consequence, they are particularly sensitive to this aqueous alteration, and more generally they are also valuable material for studying the early stage of evolution of asteroids. However, this alteration prevents the study of pristine components in matrices as they were at the time of accretion of the asteroids. Before this study, no pristine material had been described in CM chondrites, with the possible exceptions of Y-791198 (Chizmadia and Brearley, 2008) and EET 96029 (Lindgren and Lee, 2015) that were shown to have preserved good mineralogical characteristics of pristine components.

Many studies have been devoted to the mineralogical and chemical evolution during parent body alteration of the fine-grained materials in CM carbonaceous chondrites (McSween, 1979; Barber, 1981, 1985; Tomeoka and Buseck, 1985; Tomeoka et al., 1989; Zolensky et al., 1993, 1997; Browning et al., 1996; Rubin et al., 2007; see also Brearley, 2006, and Velbel and Palmer, 2011 for recent reviews). The alteration products are dominated by phyllosilicates from the serpentine group, Ca-phosphates, carbonates, tochilinite, pentlandite, sulfates and iron oxides. Several indicators have been developed to estimate the degree of alteration. They include the Fe–Mg concentration in the matrix (McSween and Richardson, 1977; McSween, 1979, 1987; Zolensky et al., 1993; Rubin et al., 2007), the abundance of Fe^{3+} (Browning et al., 1996), the bulk water/OH contents and H and N isotopes (Alexander et al., 2013), the relative abundance of phyllosilicates and anhydrous silicates (Howard et al., 2009, 2011, 2015), the level of kamacite corrosion (Palmer and Lauretta, 2011) and carbonate mineralogy (e.g., Lee et al., 2014). Phyllosilicates are the most abundant phases and are regarded by most authors as resulting from aqueous alteration of anhydrous precursor phases on the asteroid parent bodies (e.g., Brearley, 2006). It has been shown that the amount of serpentine and its chemistry is linked with the degree of aqueous alteration. As a general trend, the serpentine minerals are found to become progressively enriched in Mg as the degree of alteration increases (McSween and Richardson, 1977; Tomeoka and Buseck, 1985; Zolensky et al., 1993; Browning et al., 1996; Rubin et al., 2007). The increase of Mg content in the matrix is interpreted as a consequence of a progressive dissolution of anhydrous crystalline silicates (olivine and pyroxene) from chondrules. Regarding the early stages of alteration, the relationship of precursor phases to serpentine is still debated. The precursor material may well consist of anhydrous silicates (crystalline or amorphous), a sub-micrometer phase assemblage found in the most carbonaceous primitive chondrites (Brearley, 1993; Greshake, 1997; Abreu and Brearley, 2010; Le Guillou and Brearley, 2014).

Recently, a new CM chondrite, named Paris, was discovered. It was classified as a CM2 chondrite and is considered to be the least altered CM chondrite so far (Hewins et al., 2014). The low alteration state of the object is attested by its oxygen isotope mixing line that extends from CM2 falls toward CO3 falls. However, the range along the mixing line shows that the alteration is heterogeneous in the Paris meteorite. In the freshest areas, the metal is abundant and the matrix is dominated by amorphous material. In the more altered areas, phyllosilicates are abundant, together with the other common alteration products (magnetite, tochilinite, carbonates). Because it is less altered than most other CM chondrites, at least in some areas, Paris is a good candidate to study in details the first stages of aqueous alteration that occurred in the CM parent body and to search for pristine material in the matrix in the least altered regions. Like the most primitive carbonaceous chondrites (e.g., Acfer 094, MET 00426 and QUE 99177; Greshake, 1997: Abreu and Brearley, 2010; Le Guillou and Brearley, 2014), the less altered matrix in Paris could provide valuable information to constrain processes involved in the formation of pre-accretion fine-grained materials, as well as the first stage of alteration in the CM parent body. Hewins et al. (2014) provided an overview of the matrix mineralogy, but the detailed microstructures and submicron-sized mineralogy of fine-grained material in this chondrite have not being described to date. Here we present an analytical transmission electron microscope (ATEM) study of several areas of matrix, from relatively unaltered areas to strongly altered areas.

2. SAMPLES AND METHODS

Sections of Paris were first examined by optical microscopy and scanning electron microscopy (SEM) in order to select areas for TEM. Paris is a breccia comprising diversely aqueously altered lithologies often with ill-defined boundaries. In the freshest material, unaltered metal is abundant within chondrules, which is unique among known CMs. Suitable matrix zones for TEM were selected in various settings in the interstices between chondrule rims and, for the freshest zones, in small areas in which the lacy tochilinite growths were the least abundant. Eight electron transparent slices were prepared by focused ion beam (FIB) technique using an FEI Strata dual beam 235 at IEMN, University of Lille. Before extraction of the thin foils by the FIB, a platinum protective coating layer was deposited on the area of interest in order to minimize beam damage by the Ga ion beam. The thin foils were extracted from the petrographic section by the in-situ lift-out technique using an internal micromanipulator and were welded onto 3 mm copper TEM half grids. The sizes of the FIB sections were typically $15 \times 7\ \mu m^2$ and 100 nm thick. The FIB sections were studied by ATEM with an FEI Tecnai G2-20 TWIN (LaB_6, 200 kV) equipped with an EDAX energy dispersive spectrometer (EDS) at the electron

microscopy center of the University of Lille. The microstructure was studied by conventional bright field imaging and selected area electron diffraction (SAED). Scanning TEM (STEM) was used for acquiring EDS data, with an electron beam diameter of about 5–10 nm. The sizes of the different phases of the fine grained material were frequently less that the foil thickness (100 nm). As a consequence, many of the analyses integrate compositions of several phases along the electron beam path through the sample. Most compositional data were deduced from elemental mapping after post acquisition processing of data cubes by adding pixels in given areas of interest. This configuration helps to detect the phase overlap under the beam and allows for optimizing the localization of the individual phases, when not too small. The EDS spectra, acquired individually or extracted from chemical maps, were quantified by applying an absorption correction assuming that the FIB sections were 100 nm thick. The *k*-factor correction was applied with *k*-factors experimentally determined for the major elements (O, Mg, Fe, S, Ca and Al) with standard specimens using the parameterless correction method of van Cappellen (1990). The standards used were quartz (SiO_2) for O, forsterite (Mg_2SiO_4) for Mg, fayalite (Fe_2SiO_4) for Fe, pyrite (FeS_2) for S, diopside ($CaMgSi_2O_6$) for Ca and sillimanite (Al_2SiO_5) for Al. For minor elements (Ca, Ti, Cr, Mn, Ni), *k*-factors were calculated from the theoretical curve of the detector response to different X-ray energies, adjusted though the calibrated values of the major elements.

3. RESULTS

The microstructures studied differ significantly depending on the regions that were extracted from the Paris section. A strong variability is also found at the scale of a given FIB section, i.e. at the micro-scale. One exception is the FIB sample showing the less altered area, described in Section 3.1, for which the microstructure is quite homogeneous. This finding confirms that the degree of alteration is heterogeneous in the matrix of Paris, as noted by Hewins et al. (2014). In the following, we describe the observations based on the dominant characteristics of the samples, from the less to the more altered samples. No noticeable differences were found between samples extracted from chondrule rims and matrix. Both display similar microstructure and chemistry and so that are not distinguished in the following.

3.1. Less altered samples

In the least altered sample, the matrix is dominated by amorphous silicates. These do not form a continuous groundmass but are found as submicron sized, irregularly shaped units, separated from one another by an abundant porosity (Fig. 1a). The apparent size in the TEM section of the amorphous domains ranges from 100 nm to 1 μm, and the pore sizes range from 10 to 500 nm. The amorphous silicates units contain numerous nanometer-sized Fe-rich (Ni-poor) sulfide inclusions with sizes of a few tens of nanometers in diameter (Fig. 1b). Some S-free and Fe-rich inclusions were also detected but they are rare and their small size (below 30 nm) precludes a full characterization. No oxygen depletion is observed at the location of these Fe-bearing inclusions, thus they might be Fe-oxides. The abundance of nano-sulfide inclusions embedded in the amorphous material is heterogeneous and differs from one grain to another. Some amorphous units contain a large number of inclusions while others have none. The size of these inclusions precludes detailed composition measurements because their dimensions are well below the sample thickness and the silicates in which they are enclosed contain a significant amount of Fe. At the border of the amorphous units, a fine fibrous material is locally occasionally present (Fig. 1b). This material lacks sulfide inclusions and in some places it seems to fill entire pore spaces (Fig. 1b). Electron diffraction patterns show that it is amorphous or poorly crystalline. The corresponding compositions are close to the composition of the adjacent units. Accessory phases are found in contact with the amorphous units. They are crystalline Mg–silicates (forsterite and enstatite), Ni-rich sulfides and carbonaceous material. These minor phases are also detected in the more altered samples, and they will be described in more detail in the Section 3.5. In the least altered sample, the minor phases are located within the voids at the contact with the amorphous units.

Element and phase distributions were studied by EDS on relatively large areas like the one shown on Fig. 2a. Fig. 2b is a phase contrast image showing the distribution of the amorphous silicate domains, the Mg-rich silicates and carbonaceous material. The C-material is mostly present as patches located between the amorphous silicate units and locally rims them discontinuously. Nickel-rich sulfides are located preferentially at the rims of the silicates domains and tend to be larger, up to the few hundreds nm, compared to the Ni-poor sulfides present as nano-inclusions in the amorphous silicates. Fig. 2c is a reconstructed image showing the distribution of Fe between the amorphous phases, sulfides (Ni-rich and Ni-poor) and iron oxide. The texture of this minimally altered sample closely resembles those of GEMS (glass with embedded metal and sulfides) grains frequently found in chondritic porous interplanetary dust particles (Bradley, 1994; Keller and Messenger, 2011). Table 1 gives the mean composition of the amorphous units, including the nano-inclusions embedded within them. The average composition of the amorphous domains is not far from the CI chondritic value (for the major elements), but with a clear enrichment of Si and depletion in S. Fig. 3 shows the compositional field of the amorphous material in two ternary diagrams; Fe–Mg–Si and Fe–S–Si. The observed compositional fields are relatively narrow and centered close to the solar composition.

To estimate the porosity of the sample, we used the X-ray emission efficiency (count rate or cumulative counts) by using the EDS detector. As shown in Fig. 3, the 'GEMS-like' objects have a relatively homogeneous composition. The X-ray emission rate therefore depends only on the amount of material interacting with the electron beam. Then, we verified that the FIB sample has a roughly

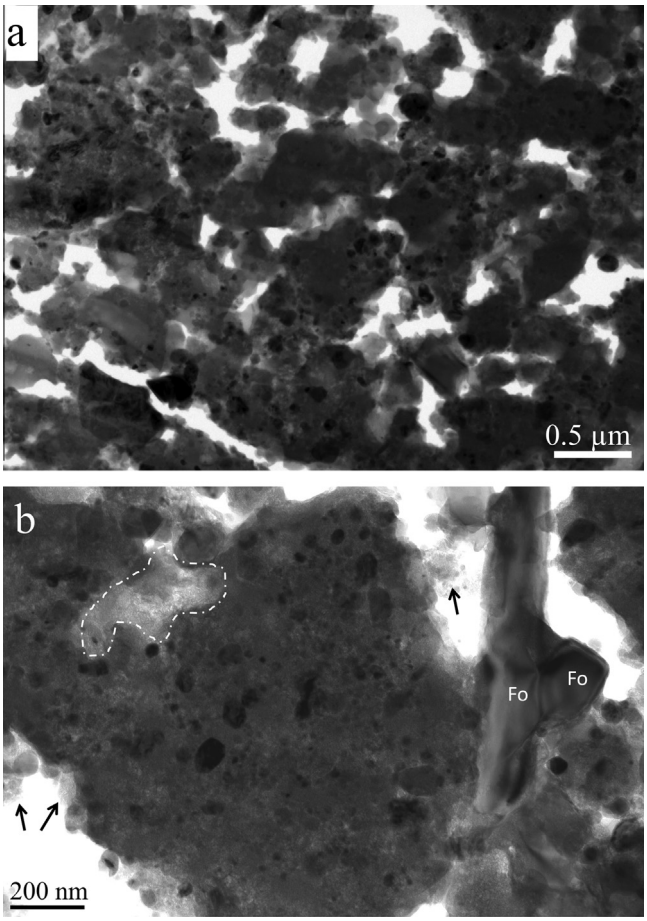

Fig. 1. Bright field TEM images of the least altered sample in Paris (a) low magnification image showing that the sample consists of amorphous units in contact with each other. There is a high porosity fraction, estimated at 30% (b) frequently, but not systematically, the amorphous domains contain abundant nano-sized opaque inclusions dominated by Fe-rich, Ni-Poor, sulfides (dark dots). Locally, fine fibrous material is present at the edge of the amorphous units. Some of them are arrowed. Some small pore spaces are fully filled by a very fine fibrous material (surrounded by a white dashed line). Two grains of forsterite are present (Fo). One has a needle shape with an apparent size of $\sim 1.1 \times 0.2$ µm. The other adheres to the needle with a clean grain boundary.

uniform thickness. This was done by measuring the X-ray emission rate at the center of several amorphous grains, where there is no porosity. The proportion of porosity has been deduced by measuring the X-ray emission rate on the entire sample. It was inferred using a linear proportionality rule between the compact material (no porosity and a given level of X-ray emission) and the empty space (full porosity, no X-ray emission). We derived from these measurements that the average porosity of this sample was approximately equal to 30%.

3.2. Moderately altered areas

Most of the samples studied display clear evidence of aqueous alteration. In moderately altered areas, the microstructure consists of a mixture of amorphous silicates, frequently with a mottled contrast, and very fine-grained fibrous material having a spaghetti-like morphology. The amorphous material contains abundant nano-sized sulfide inclusions, both Ni-poor and Ni-rich. The nano-sulfide inclusions are absent from areas where the fibrous texture is clearly apparent. The fine-grained fibrous material is heterogeneously distributed in small pockets (Fig. 4a). It probably formed within the porosity network that was described in the previous paragraph for the least altered sample. As a general trend, the porosity volume and the number of sulfide nano-inclusions tend to decrease as the abundance of fine-fibrous material increases (Fig. 4b and c). In some samples, the amorphous material and the fine-fibrous material form a continuous groundmass without porosity (Fig. 4d). In this case, the fibrous texture tends to be coarser. Depending on the sample, it seems that there is a continuous gradation between a sample dominated by amorphous domains (containing nano-sulfide inclusions and porosity) and samples dominated by a fibrous texture (without nano-sulfide inclusions and without porosity). Fig. 5 shows selected area electron diffraction (SAED) patterns from the fully amorphous material to the well-developed fibrous material. The fine-grained fibrous material is very poorly crystalline (Fig. 5b). The corresponding SAED pattern shows two weak and broad rings with *d*-spacings of 2.6 Å and

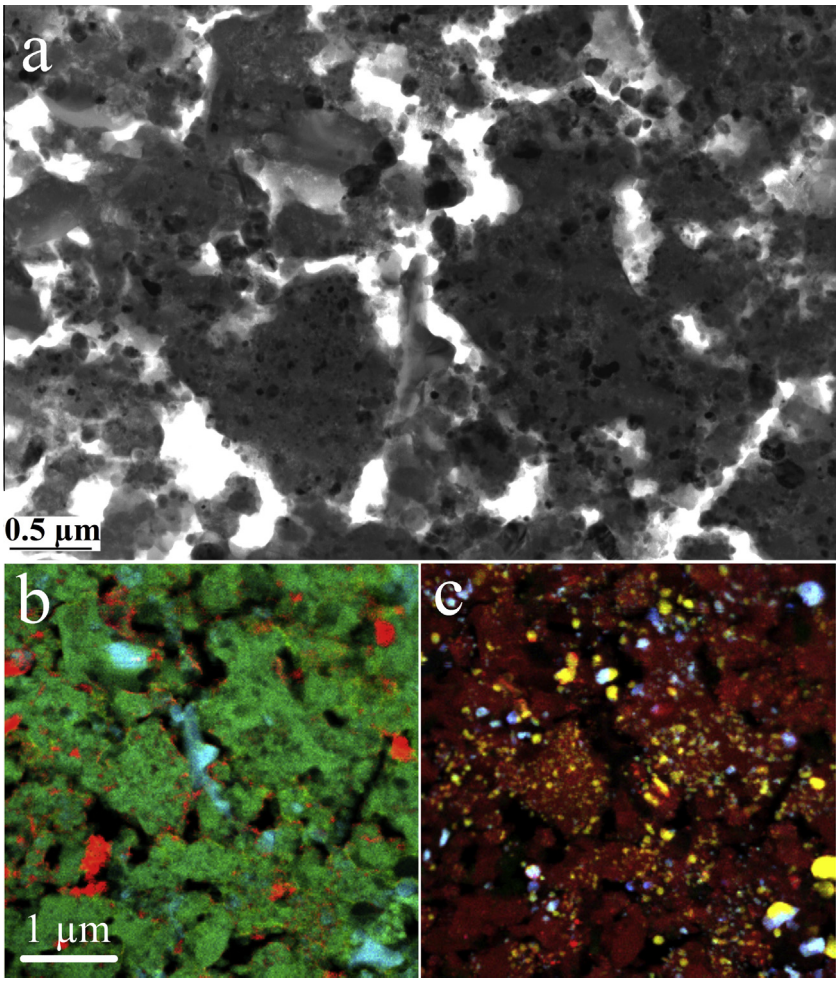

Fig. 2. Chemical mapping of the less altered material (a) bright field TEM image of the amorphous silicate domains, from part of which chemical map has been obtained (b) RBG phase contrast image on the same area, with the amorphous silicate in green, the Mg-rich silicates in blue and the carbon material in red. Note that some of amorphous units are rimmed with a thin discontinuous layer of carbon material. (c) RBG image highlighting the distribution of Fe within the different phases: amorphous material (brown), Fe-poor sulfides (yellow), Ni-rich sulfides (light blue) and iron oxide (red). (For interpretation of the references to colour in this figure legend, the reader is referred to the web version of this article.)

1.54 Å. These rings originate from randomly oriented nanocrystallites. Because of their weakness and broadness, it is difficult to identify the origin of the rings. Such a two-ring structure has already been found in altered silicates in carbonaceous chondrites and was interpreted as being consistent with 2-line ferrihydrite (Janney et al., 2000; Abreu and Brearley, 2010). However it could also correspond to the early formation of cronstedtite-1T (space group $P31m$; Hybler et al., 2000) that displays strong reflections for these d-spacings. With coarsening of the fibrous texture, the two rings at 2.6 and 1.5 Å are stronger and additional rings appear at 3.6, 4.6 and 5.2 Å (Fig. 5c). The rings cannot be identified unambiguously, but they are compatible with cronstedtite-1T for the 3.6 and 4.6 Å rings (respectively 002 and 100 reflections) and tochilinite for the reflections at 5.2 Å.

The amorphous areas have a chemical composition that is very close to the "GEMS-like" units previously described from the less altered material. In areas that have developed a fine-fibrous texture, the composition tends to be richer in Fe. These areas do not contain any apparent sulfide nano-inclusions. However, sulfur is still present in the EDS spectra, suggesting that S could be present in fibrous tochilinite mixed with fibrous silicates. The occurrence of tochilinite in the fibrous material is suggested by SAED results, as discussed above. Due to the very fine scale of the material, it was not possible to confirm this occurrence with our instrument. Average chemical compositions of the fine-fibrous material are given in Table 1. Fig. 6a shows the compositional field in the ternary diagram Fe–Mg–Si of a partly altered sample consisting of a mixture of amorphous silicates and fine-grained fibrous material. The corresponding texture is shown in Fig. 4d. The compositions are roughly aligned along a line that joins a composition close to CI carbonaceous chondrites, corresponding to areas which are amorphous, to more Fe-rich compositions for fibrous areas. Fig. 6b includes analyses extracted from several samples with a fine-grained fibrous texture. In all samples, the

Table 1
Average atomic element composition, normalized to Si, and standard deviations (in italics) of the different morphologies studied for the major elements Mg, Fe, S, Al, Ca and Ni. The GEMS-like objects correspond to the least altered material studied shown in Figs. 1–3. For the fibrous material, present in abundance in the other samples, they are classified according to their apparent morphology (from amorphous, to fine and coarse-grained material). The average compositions of GEMS in CP-IDPs and in micrometeorites, of the amorphous silicate material in Acfer 094 and CI are shown for comparison.

	Mg/Si	Fe/Si	S/Si	Al/Si	Ca/Si	Ni/Si
GEMS-like objects, $N = 90$	0.71	0.68	0.29	0.06	0.012	0.05
	0.17	*0.19*	*0.20*	*0.03*	*0.010*	*0.04*
Mixture of Amorphous and fine-grained fibrous material, $N = 339$	0.60	0.76	0.16	0.06	0.005	0.04
	0.10	*0.21*	*0.08*	*0.02*	*0.003*	*0.02*
Fine to coarse-grained fibrous material, $N = 94$	0.56	1.22	0.17	0.06	0.03	0.06
	0.08	*0.25*	*0.08*	*0.02*	*0.02*	*0.02*
Coarse-grained fibrous material, $N = 93$	0.68	2.20	0.53	0.10	0.02	0.05
	0.26	*0.73*	*0.34*	*0.03*	*0.01*	*0.02*
Platy Cronstedtite, $N = 81$	0.53	1.61	0.07	0.20	<0.01	0.02
	0.13	*0.31*	*0.05*	*0.07*	–	*0.02*
GEMS in IDPS (a)	0.67	0.56	0.30	0.07	0.04	0.03
GEMS in UCAMMs (b)	0.81	0.53	0.60	0.06	0.04	0.04
GEMS in CP MMs (c)	0.86	0.66	0.16	0.10	0.04	0.04
Acfer 094 (d)	0.48	0.98	0.15	0.07	0.05	0.05
CI Chondrite composition (e)	1.03	0.87	0.44	0.083	0.060	0.048

(a) Average composition of GEMS grains in CP-IDPs, from Keller and Messenger, 2011. (b) GEMS in ultracarbonaceous micrometeorite (UCAMM), from Dobrica et al. (2012). (c) GEMS in chondritic porous micrometeorites (CP MMs) in the surface snow and blue ice of Antarctica, from Noguchi et al. (2015). (d) Amorphous silicates in Acfer 094, from Keller and Messenger (2012). (e) CI composition, from Lodders (2010).

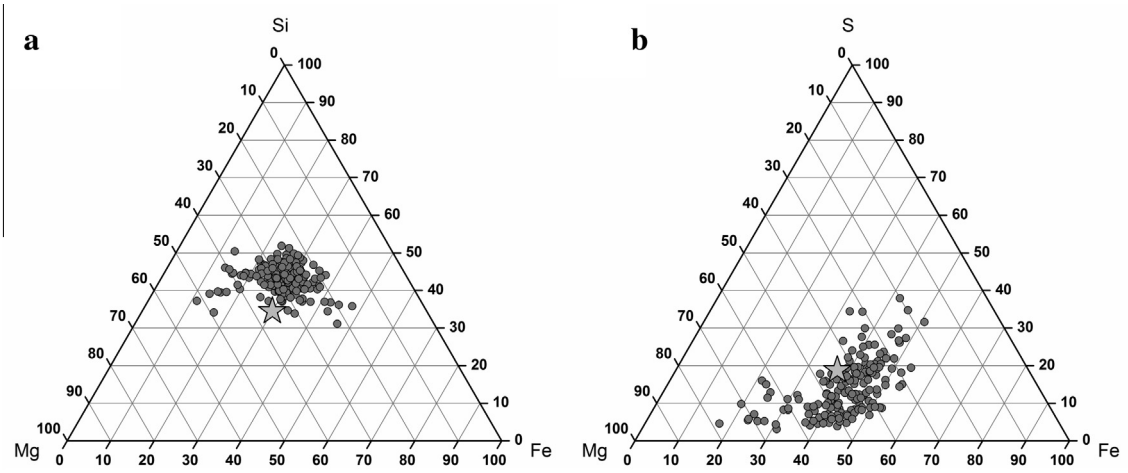

Fig. 3. Composition fields (at.%) of the amorphous material from the less altered matrix material in Paris (number of analyses $N = 174$). The compositions include the embedded nanosulfides (a) in the ternary diagram Fe–Mg–Si (b) in the ternary diagram Fe–Mg–S. The CI composition is indicated by a star (data from Lodders, 2010). Note that the compositions display, on average, enrichment in Si and depletion in S when compared to the CI composition. The data were extracted from chemical maps. The selected area was 200 × 200 nm^2 in size for each point. Data are given in at.%.

compositions of the partially altered matrix are aligned along a line that joins the bulk composition of the matrix to the Fe apex. The Mg/Si ratio is independent of the texture, suggesting that its evolution is closely related to the mobility of Fe during these first stages of alteration.

3.3. More severely altered areas

In the more severely altered areas, the fibrous texture is coarser (Fig. 7). These coarse-grained morphologies can be found in contact with amorphous to fine-grained textures, showing a strong heterogeneity of the texture at the micron-scale (Fig. 7a). In these coarse grained fibrous regions, the nanosulfide inclusions are absent but relatively coarse Fe or Fe–Ni sulfides are found, which have a size of a few hundreds of nm (Fig. 7b). For the coarser texture, Bragg contrast is clearly visible showing that the fibers are well crystalline. The SAED patterns display strongly elongated spots with *d*-spacings of 7.2, 4.6 and 3.6 Å, typical of cronstedtite, frequently associated with a reflection at

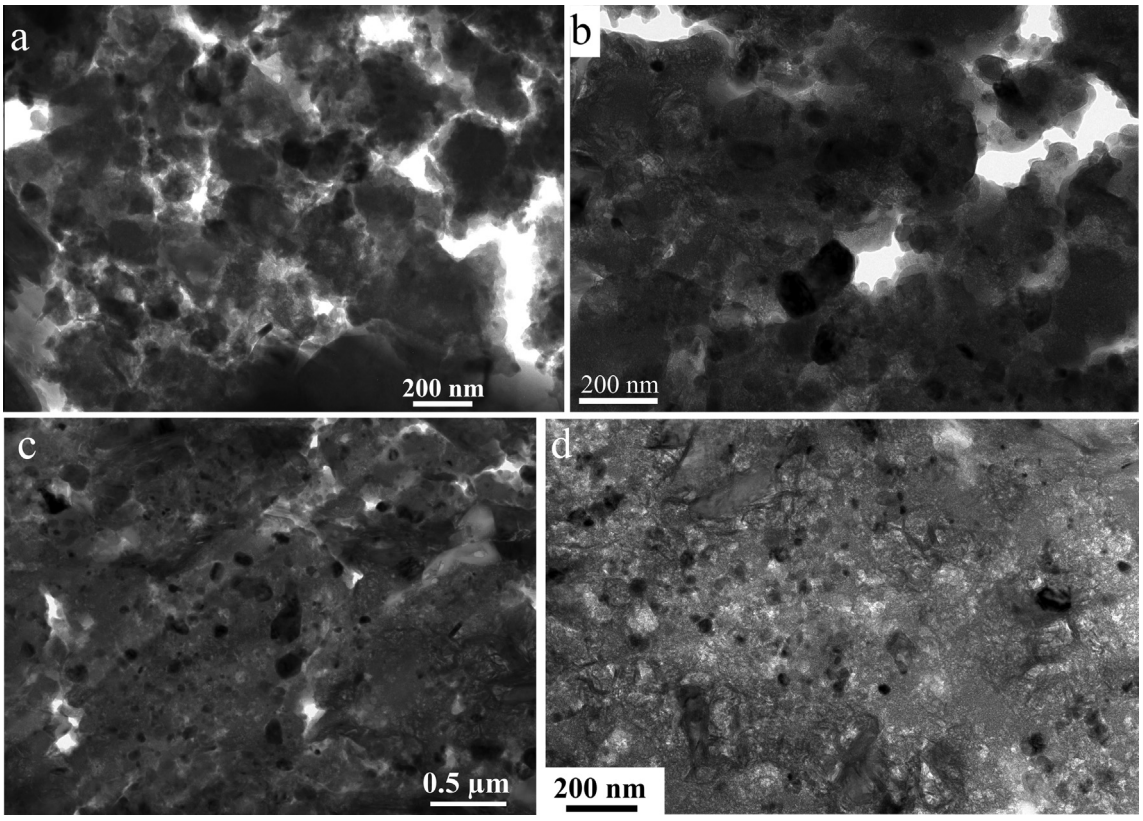

Fig. 4. Bright field TEM images of partially altered matrix areas composed of a mixture of amorphous and fine-fibrous materials. (a) In the weakly altered areas, the fine-fibrous material is located within interstices between the amorphous domains. (b and c) When the fibrous material fraction increases, the porosity decreases. (d) When the porosity is filled with fibrous material, the amorphous material and the fine fibrous silicates form a continuous groundmass.

5.2 Å, which is likely to be attributable to tochilinite (Fig. 5d). The average composition of the coarse-grained fibrous areas is Fe-rich (Table 1). Fig. 8 shows the compositional field of the coarse grained material in the ternary diagram Fe–Mg–Si. Compared to the fine-fibrous material (Fig. 6), the compositional field is shifted toward the Fe apex. As for the fine fibrous material, significant S is found in the EDS spectra, suggesting the presence of fibrous tochilinite intermixed with the fibrous silicates.

3.4. Platy cronstedtite

In the following, we used the term 'cronstedtite' to refer to the Fe-rich serpentines, although they contain significant Al and Mg. Large cronstedtite crystals are commonplace (Fig. 9). They are present in all the samples except the least altered one containing 'GEMS-like' units that is described in Section 3.1. The cronstedtite grains have a platy morphology and are generally elongated and up to several micrometers in length (Fig. 9). They are confirmed as cronstedtite according to their stoichiometry, their high Fe concentration and their electron diffraction signature. Compositions differ between grains from grain to grain (Fig. 9 which shows the compositional field in the ternary diagram Fe–Mg–Si). The Mg/(Mg + Fe) values range from 0.40 to 0.15, and the stoichiometry suggests the presence of trivalent Fe. Table 1 gives the average composition for a population of 81 grains, as well as the standard deviation. Based on a total of 5 cations (2 on the tetrahedral sites and 3 on the octahedral sites), the average cronstedtite structural formula can be written as $(Mg_{0.27}Al_{0.05}Fe_{0.68})_3(Si_{0.75}Al_{0.07}Fe_{0.18})_2O_5(OH)_4$, assuming an equal distribution of Al on the tetrahedral and octahedral sites. This cation distribution requires 15% and 85% of Fe on the tetrahedral and octahedral sites, respectively. Based on the stoichiometry and the charge balance between the tetrahedral and octahedral sites, the Fe^{3+} content in cronstedtite is estimated at 33% of the total iron. Cronstedtite can be found in contact with amorphous or fine-fibrous material. It seems that the platy grains have filled porosity that was initially present in the sample (Fig. 9a and b). In contrast to the fibrous phyllosilicates, there is no evidence that the cronstedtite originated from an alteration of the amorphous material. When the two phases are present together, they display sharp interfaces and lack clear evidence of replacement. Locally, the platy cronstedtite is replaced by fibrous material with a related orientation, suggesting an alteration of the platy grains (Fig. 9c). Cronstedtite grains are frequently interlayered with tochilinite, as identified by SAED (Fig. 9d) and qualitatively by EDS. The *c*-axis of tochilinite is found to be parallel to the *c*-axis of cronstedtite (Fig. 9d). The Mg/(Mg + Fe) ratio of tochilinite is

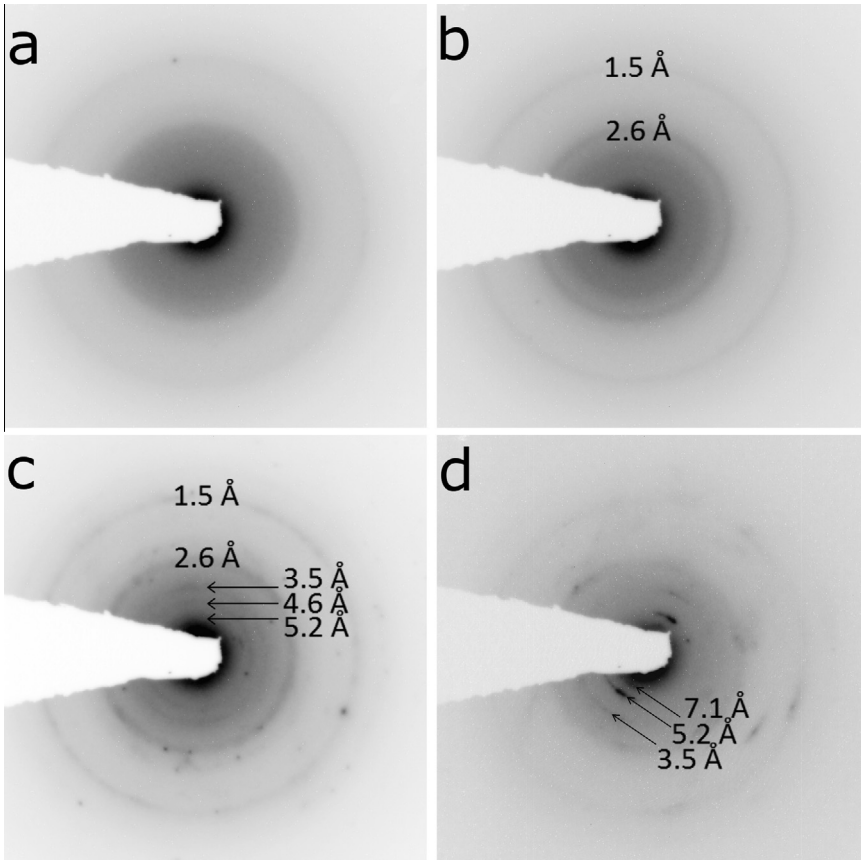

Fig. 5. SAED patterns collected from areas having different textures, classified here by their degree of alteration. For all the SAED patterns the selected area aperture was 200 nm in diameter (a) amorphous material with its characteristic diffuse rings. (b) Very fine-grained fibrous material shows more or less intense broad rings with *d*-spacings close to 2.6 and 1.5 Å. (c) Coarser fibrous material showing additional rings at 3.5, 4.6 and 5.2 Å. (d) The coarse-grained fibrous texture, shown on Fig. 7a, with reflections at 3.5, 5.2 and 7.1 Å. The spot streaking is related to the curved morphology of the phyllosilicates.

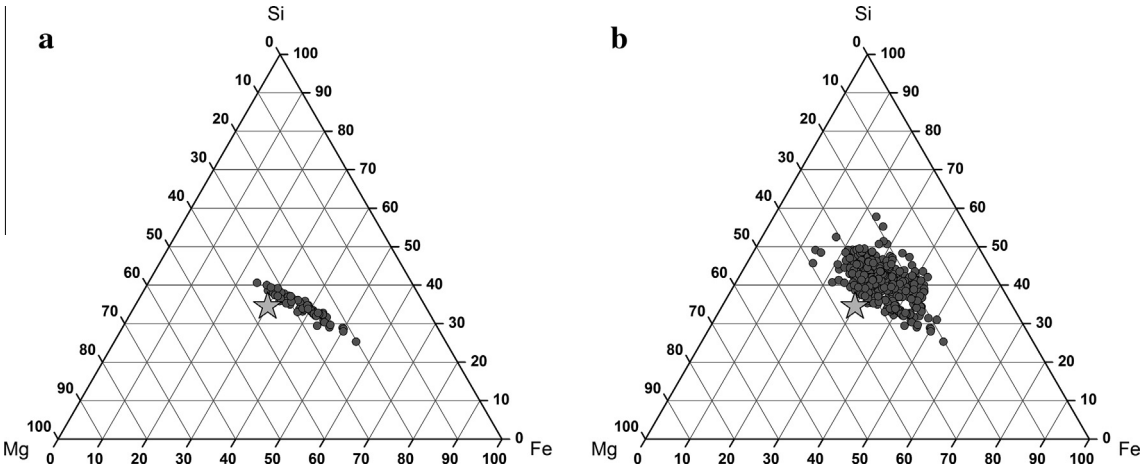

Fig. 6. Composition field in the ternary diagram Fe–Mg–Si of partially altered material, consisting of a mixture between amorphous and fine-grained fibrous material (at.%). All data were extracted from chemical maps (a) composition field of the area shown in Fig. 4d. Each value corresponds to a 300 * 300 nm^2 area extracted from the post-acquisition processing of a chemical map ($N = 65$). The total surface area analyzed was 2.5 * 2.5 μm^2. The composition field is relatively narrow but is strongly elongated from approximately the CI value in the direction of the Fe apex. As a general trend, the areas dominated by amorphous material have a composition close to CI while the fine-fibrous material is enriched in Fe. Note that the Si/Mg ratio is still approximately constant (b) data collected on different samples, for surface areas from 200 * 200 nm^2 to 300 * 300 nm^2 for each point ($N = 405$). On average, the compositions show an enrichment of Si and Fe compared to the CI value. As for (a), when the fibrous material is dominant, the compositions are shifted to the Fe apex.

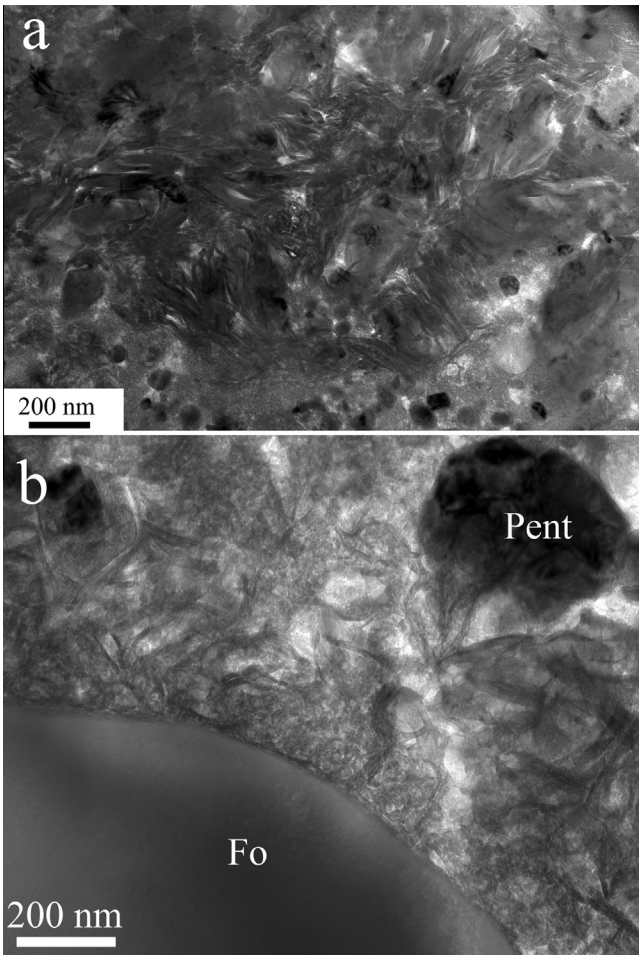

Fig. 7. Bright field TEM image of coarse grained fibrous areas. (a) Coarse-grained, spaghetti-like, region. Note the presence of nano-sulfide inclusions in the bottom in a region consisting of a mixture between amorphous material and fine-fibrous material. These nano-inclusions are not present within the coarse grained fibrous material (b) fibrous areas in contact with a large pure forsterite grain (Fo). There is no sign of forsterite alteration, as illustrated by the clean curved grain margin. A pentlandite crystal is also present (pent).

close to 0.3 (only a few large grains have been analyzed) Fig. 10.

3.5. Minor phases and phase distribution

All the samples studied, whatever their degree of alteration, contain crystals of forsterite and enstatite, in approximately equal quantities and sizes (25 forsterite and 30 enstatite grains have been analyzed). Compositions are reliable only for crystals with a size greater than the thickness of the FIB sections (100 nm). For small grains, below 100 nm, the EDS spectra display some Fe due to the beam overlap with the surrounded Fe-rich silicate groundmass. These anhydrous crystalline silicates are all pure or almost pure Mg–silicates. They show compositions within the range $Fo_{98\text{-}100}$ and $En_{98\text{-}100}$. A few Fe-free diopside grains were also detected. Whatever the studied areas (altered or not), the distribution of minor elements (Al, Ca, Cr and Mn) in the Mg–silicates is highly variable, suggesting that they have various origins. Representative compositions are given in Table 2. In the less altered areas (containing amorphous material with nano-sulfide inclusions), the Mg–silicate grains are, on average, smaller and irregularly shaped. In contrast, in the altered areas (containing fibrous silicates) the Mg–silicates are larger, on average, with a rounded interface with the fibrous material (Fig. 11; see also Fig. 11a in Hewins et al., 2014) and grains with sizes lower than 100 nm are not present. Some of the crystalline Mg–silicates are elongated, both for forsterite and enstatite (Fig. 2a and 11c). For enstatite, the direction of elongation is along the [100] axis and the crystals contain numerous staking faults in the (100) plane. This morphology and microstructure resembles that of enstatite whiskers which are abundant in CP-IDPs (Bradley et al., 1983). We only detected a few of these grains, but they are probably more abundant because the FIB sectioning gave a low probability of having the needles in the plane of the FIB section. The forsterite grains are free of crystal defects or inclusions. A majority of the forsterite and enstatite grains have a clean interface with the surrounding silicate groundmass, whatever the alteration degree of the region in which they are enclosed, showing that there was no interaction with the

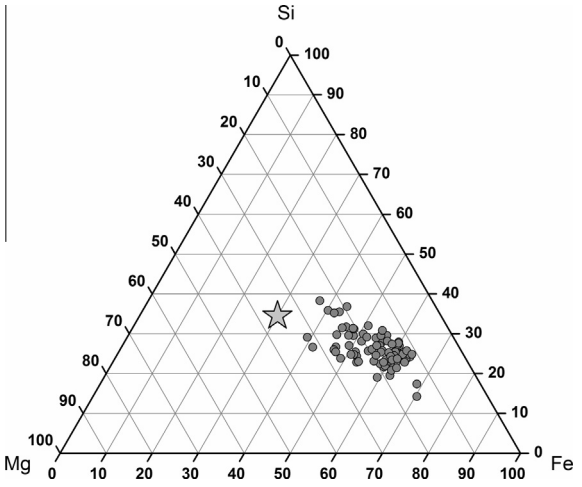

Fig. 8. Composition field in the ternary diagram Fe–Mg–Si of coarse-grained fibrous material (at.%). Compared to the fine-fibrous material shown on Fig. 6b, the composition field is shifted toward the Fe apex. Data were extracted from several composition maps and individual analyses. Each analysis corresponds to an analyzed surface area of 300 * 300 nm^2 ($N = 93$).

surrounded silicate groundmass, even when the latter is composed of phyllosilicates. However, a few enstatite grains display clear evidence of partial alteration by interaction the surrounding matrix (Fig. 11c). In this case, the crystalline silicate is locally replaced by an Fe-rich fibrous material. The addition of Fe illustrates the high iron mobility in the silicate groundmass. It also suggests that enstatite is less resistant to replacement than forsterite.

All the FIB samples also contain carbon-rich globules (Fig. 12). These globules closely resemble those found in a number of carbonaceous chondrites (e.g., Garvie and Buseck, 2004; Nakamura-Messenger et al., 2006; Abreu and Brearley, 2010; De Gregorio et al., 2013; Le Guillou and Brearley, 2014), in Wild 2 samples (De Gregorio et al., 2010) and in micrometeorites or IDPs (Matrajt et al., 2012). They have a rounded shape and frequently show a central hole. Some carbonaceous grains are strongly elongated, lacey-shaped (Fig. 12c). Carbon phases that are smaller in size are also detected in chemical maps of all the samples. This carbon is often present in the form of thin filaments in the interstices of the other phases (Figs. 2 and 13). In the less altered material described in Section 3.1, the carbonaceous material is in contact with the amorphous silicate units as small pockets or rims discontinuously coating the units (Fig. 2).

Other minor phases are rare. We detected several small Ca-phosphate grains (<100 nm in size). On chemical maps, some tiny Ca-rich grains are also detected, but they do not correlate with P or C suggesting that they are not associated with Ca-phosphate or carbonates. They could be Ca-rich pyroxene but their small size (typically 10–20 nm), well below the thickness of the samples (100 nm), precluded individual composition measurements without overlap with the surrounding phases. We have also detected some small spots of Al and Cr without being able to identify the corresponding phases.

These minor phases represent only a small proportion of the material in the matrix which is dominated by amorphous silicate, partially or completely transformed into fibrous phyllosilicates. The distribution of the different phases (amorphous or fibrous silicates, anhydrous crystalline Mg–silicates, sulfides and carbonaceous material) can be visualized in chemical maps, especially RGB phase contrast images (Fig. 13). These maps also highlight the heterogeneity of the samples in terms of the intensity of alteration, even at the micrometer scale. For instance, the amorphous to finely fibrous material (containing many sulfide inclusions) can be found in contact with coarse-fibrous material (without sulfide inclusions) with a sharp interface between the two (Fig. 13). They also show the distribution of Fe between the different phases, highlighting the two populations of sulfides (Ni-poor and Ni-rich) and the Fe-enrichment in the fibrous material compared to the amorphous material. Tochilinite fibers (dark blue and greenish in C–Mg–Si and Fe–Ni–S, respectively) intimately admixed with fibrous phyllosilicates but absent from the amorphous material (Fig. 13a). A large grain of cronstedtite (deep red) in the fibrous material contains oriented layers of tochilinite, explaining the S content reported for this silicate mineral (Hewins et al., 2014). In general, the coarse fibrous regions (light red in the Fe–Ni–S images of Fig. 13) contain less carbonaceous material compared to the amorphous of finely fibrous material (red–brown).

4. DISCUSSION

Numerous TEM studies have been devoted to fine-grained CM chondrite matrices (e.g., Barber, 1981, 1985; Tomeoka and Buseck, 1985; Lauretta et al., 2000; Zega and Buseck, 2003, see also the recent review by Velbel and Palmer, 2011). They have shown that these matrices are made up of fine-grained components, dominated by phyllosilicates that were produced by extensive aqueous alteration in their parent body. Our study of the matrix of Paris also shows strong evidence for aqueous alteration, as attested by the presence of phyllosilicates. Nevertheless, the matrix also contains abundant amorphous silicates. Some regions have escaped aqueous alteration to some extent and thus have preserved locally pristine characteristics. The discussion first focuses on the heterogeneity of the microstructure. The second part is devoted to the least altered material in order to place it in the context of primitive objects of the Solar System that have already been identified. In the third part, the diversity of the microstructure is used to define the mineralogical evolution associated with the earliest stages of aqueous alteration in the Paris parent body.

4.1. Paris, a heterogeneously altered CM chondrite

Recently, Hewins et al. (2014) described the meteorite Paris as the least altered CM chondrite discovered so far. The low degree of alteration is shown by the abundance of metal in a number of regions of the meteorite. The oxygen isotope mixing line extends from CM2 falls toward CO3 falls, showing that Paris is less altered than the other

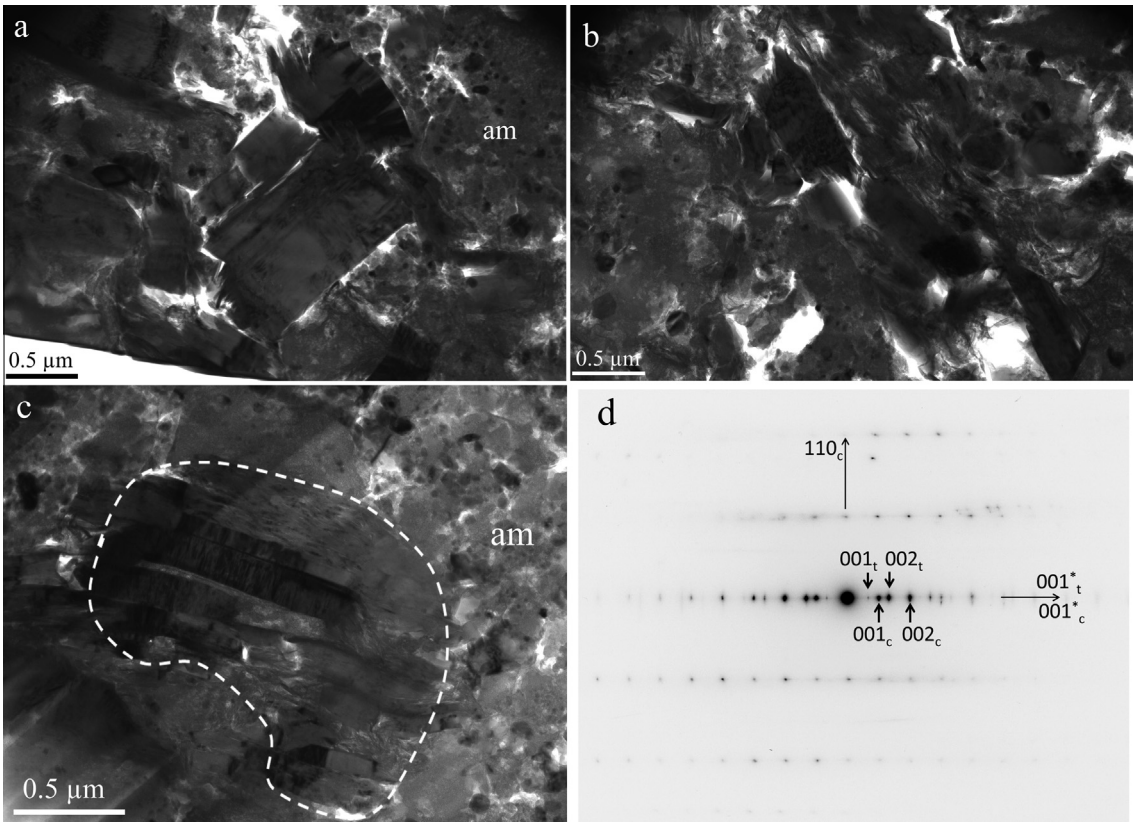

Fig. 9. Bright field TEM images and diffraction data of cronstedtite grains. (a) Several cronstedtite grains having different crystallographic orientations. They seem to fill porosity initially present in the pristine assemblage. The cronstedtite grains are in contact with an amorphous region containing number of nano-sulfide inclusions (right side of the image, labeled 'am') (b) mixture of cronstedtite grains and coarse-grained fibrous material, in contact with a fine-fibrous region on the bottom-left part. (c) Pocket of cronstedtite interlayed with tochilinite, delimited by a dashed white line. The area is strongly crystallographically oriented. Small pockets of fibrous material are locally present and the orientation of the fibers seems related to the crystallographic orientation of cronstedtite. The cronstedtite region is in contact with some of the least altered material consisting of a mixture of amorphous material (labeled 'am') and fine-fibrous material (right side on the image). (d) Selected area electron diffraction pattern recorded from a cronstedtite crystal (labeled 'c') containing a thick tochilinite (labeled 't') interlayer. The two phases share the same orientation for their *c*-axis.

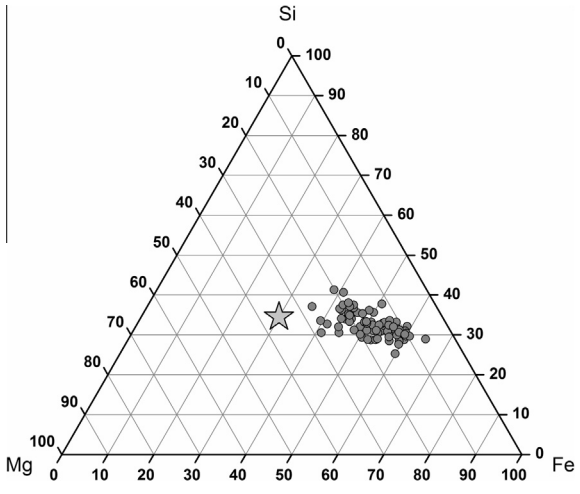

Fig. 10. Composition field of the platy cronstedtite crystals in the Fe–Mg–Si ternary diagram (at.%) ($N = 81$). The average composition is given in Table 1.

CM chondrites. However the extent of the mixing line is large because of local alteration heterogeneities. If some regions of the meteorite are fresh, others display clear evidence of significant alteration as indicated by the presence of Ca-carbonates, magnetites and corrosion rims around large metal grains. Using the PCP index of Rubin et al. (2007) and Hewins et al. (2014) showed that the PCP clumps have a moderate alteration index. They deduced a petrographic subtype ~2.9, making this meteorite the least altered CM chondrite discovered so far. For Marrocchi et al. (2014), Paris should be classified as type 2.7. These slight discrepancies are certainly linked with the strong heterogeneity of the CM Paris sample.

In CM chondrites, strong variations in alteration intensity have been already reported (e.g., McSween, 1979; Zolensky et al., 1997; Lauretta et al., 2000; Beck et al., 2010). The present TEM study confirms the high degree of heterogeneity of the microstructure demonstrating that Paris experienced varying degrees of aqueous alteration, even at the micrometer scale. This heterogeneous alteration suggests that the primitive material of Paris, despite its high

Table 2
Selected EDS analyses of anhydrous silicates (at.%). Data are normalized to 100% and were quantified using the procedure given by van Cappellen and Doukhan (1994). Uncertainties for the major elements (O, Mg and Si) are typically 3%, and those for the minor elements (<0.5 at.%) are typically 20%.

	O	Si	Mg	Al	Ca	Ti	Cr	Mn	Fe	
Forsterite #1	56.7	13.3	29.7	nd	nd	nd	0.06	0.10	0.07	Fo_{100}
Forsterite #2	57.2	14.3	27.7	nd	nd	nd	0.11	0.23	0.40	Fo_{99}
Forsterite #3	57.4	14.7	27.9	nd	nd	nd	nd	nd	0.03	Fo_{100}
Enstatite #1	60.1	20.2	19.7	nd	nd	nd	nd	nd	nd	En_{100}
Enstatite #2	59.7	19.2	20.0	0.16	0.48	nd	0.18	0.20	0.14	En_{99}
Enstatite #3	59.5	19.2	18.4	0.35	1.52	nd	0.28	0.43	0.26	En_{99}
Diopside #1	60.4	20.0	9.54	1.76	8.08	nd	nd	nd	0.05	$Wo_{46}En_{54}$
Diopside #2	59.9	17.4	11.3	4.88	6.19	0.03	nd	nd	0.23	$Wo_{35}En_{64}$

porosity, has not been percolated by fluids in a pervasive way, in agreement with the estimated low permeability due to the fine grain size of primitive matrices of carbonaceous chondrites (Bland et al., 2009). The least altered samples are those containing amorphous material that has a large number of Fe-sulfide nano-inclusions. In more altered regions, a fibrous microstructure has developed gradually, reflecting the nucleation and growth of phyllosilicates. The chemical signature of the matrix is also found to evolve significantly in direct relationship with the microstructure, suggesting local continuous chemical exchange of the matrix with aqueous fluids.

4.2. Pristine material well preserved in the Paris matrix

In Figs. 1–3 we documented amorphous sub-micron sized silicates domains, nano-inclusions of Fe-sulfides and a high porosity (~30%). These characteristics, along with the absence of phyllosilicates, shows that this "least altered" matrix was not significantly aqueously altered or thermally processed. Indeed, amorphous silicates are known to be highly metastable and therefore highly reactive with the environment. When they interact with water, amorphous silicates are easily transformed into phyllosilicates, even at low temperature (e.g., Rietmeijer et al., 2004; Chizmadia et al., 2006; Nakamura-Messenger et al., 2011). Sulfides are also sensitive to aqueous alteration and thermal metamorphism, especially when the grains are so small (Grossman and Brearley, 2005; Abreu and Brearley, 2010; Palmer and Lauretta, 2011). Sulfur is highly mobile in matrices, redistributed either by diffusion or transportation in S-rich fluids. The presence of porosity (30%) is also a valuable indication that alteration is absent or weak. The infiltration and circulation of fluids throughout open spaces would have filled them by deposition of dissolved species, forming secondary phases such as PCPs for instance (e.g., Trigo-Rodriguez et al., 2006).

The amorphous material in Paris has much in common with that of the most primitive material, such as the GEMS grains in CP (chondritic porous)-IDPs (Bradley, 1994; Keller and Messenger, 2011), in ultracarbonaceous micrometeorites (Dobrica et al., 2012), in CP micrometeorites (Noguchi et al., 2015) and with the silicate groundmass of matrices in the primitive chondrites ALHA77307 (Brearley, 1993), Acfer 094 (Greshake, 1997) and the CR3.0 chondrites QUE 99177 and MET00426 (Abreu and Brearley, 2010; Le Guillou and Brearley, 2014). It contrasts significantly with most of the other CM chondrites and the more altered areas in Paris for which phyllosilicates are the major phase. A possible exception is the CM Y 791198, studied by Chizmadia and Brearley (2008), for which there are strong analogies in the microstructure. However, the porosity is absent in the CM Y 791198 and the composition of the matrix is more enriched in Fe. Table 1 gives a comparison between the chemistry of the fresh matrix of Paris with previously known primitive materials (GEMS in IDPs, GEMS in micrometeorite and the amorphous material in primitive chondrites) for the most abundant elements (Si, Mg, Fe, S, Ca, Al, Ni). As for GEMS in IDPS and micrometeorites, the average composition of the GEMS-like objects in Paris is close to the solar value, but with a noticeable enrichment in Si. In Fig. 14, the compositional field of the GEMS-like objects in Paris is plotted in the ternary diagram Fe–Mg–Si, together with the corresponding composition field of GEMS in IDPs (data from Keller and Messenger, 2011) and that of the Acfer 094 chondrite (data from Leroux et al., 2014). A direct comparison is made possible here because the compositional data were acquired with a similar methodology, in a TEM. For each composition, the analyzed volume is comparable (approximately 200 × 200 nm, for TEM samples about 100 nm thick). The comparison of the three compositional fields reveals significant differences. The GEMS in IDPs and the GEMS-like objects of Paris have comparable average compositions, but the composition field of the GEMS in IDPs is much larger. This difference is possibly due to a chemical homogenization in the Paris parent body or due to the fact that GEMS grains in IDPs sample a large range of dust from the solar nebula, while the material in Paris could originate from a much smaller area with chemical properties that were specific to the region from which the Paris parent body accreted. Compared with the GEMS in IDPs and Paris, the compositional field of the amorphous silicates of Acfer 094 is clearly shifted toward the Fe-rich region. The Acfer 094 amorphous silicates are also depleted in S and Ca compared to the CI composition (Keller and Messenger, 2012; Leroux et al., 2014). These chemical signatures are likely the consequence of moderate aqueous alteration on the parent body, oxidation reactions involving metal and sulfides and further redistribution of

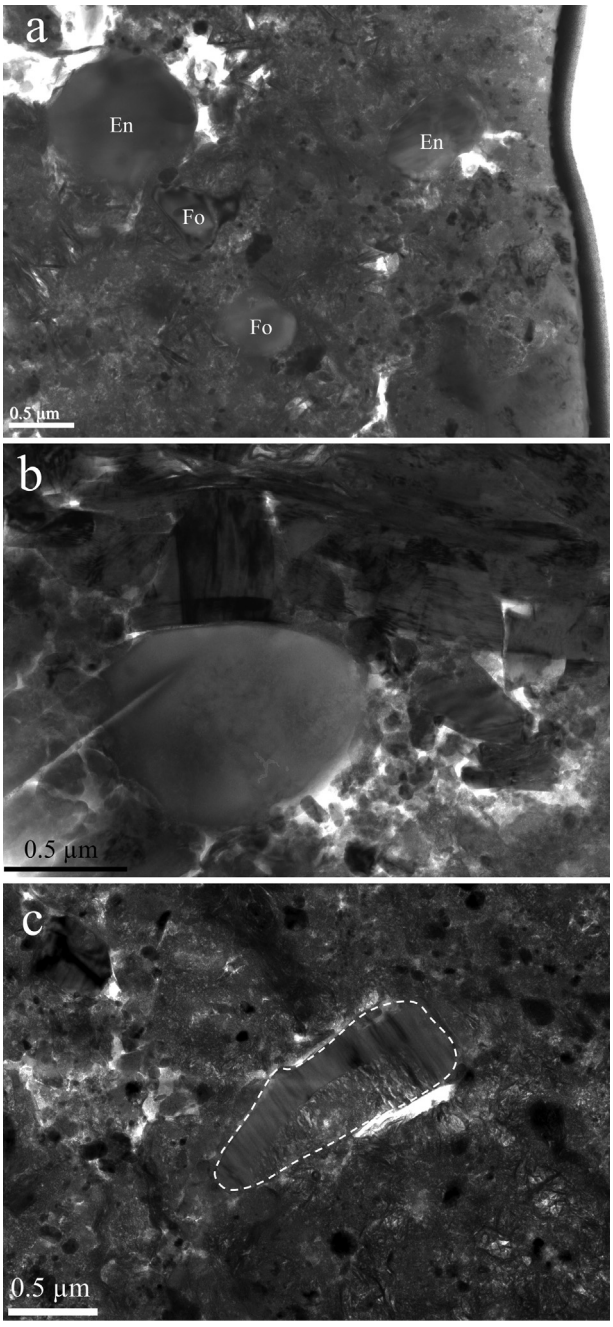

Fig. 11. Anhydrous Mg–silicates in the matrix, TEM bright fields images. (a) Forsterite and enstatite grains distributed within the matrix (here dominated by a mixture of fine to coarse grained fibrous silicates). Note the rounded shape of the grains. (b) Rounded forsterite in contact with cronstedtite. The interface between the two phases is abrupt and there is no composition gradient on either side. (c) Enstatite grain showing evidence of interaction with the surrounding matrix material, here transformed into phyllosilicate. The composition of the replacement matter is Fe-rich, showing that Fe is highly mobile. The original shape of the enstatite grain is retained, as indicated by the elongated shape of the crystal along the [1 0 0] axis. The surrounding matrix is made of fine fibrous to coarse fibrous material. Some iron sulfide nano-inclusions (dark dots), as well as a few porous areas, are still present despite the altered texture.

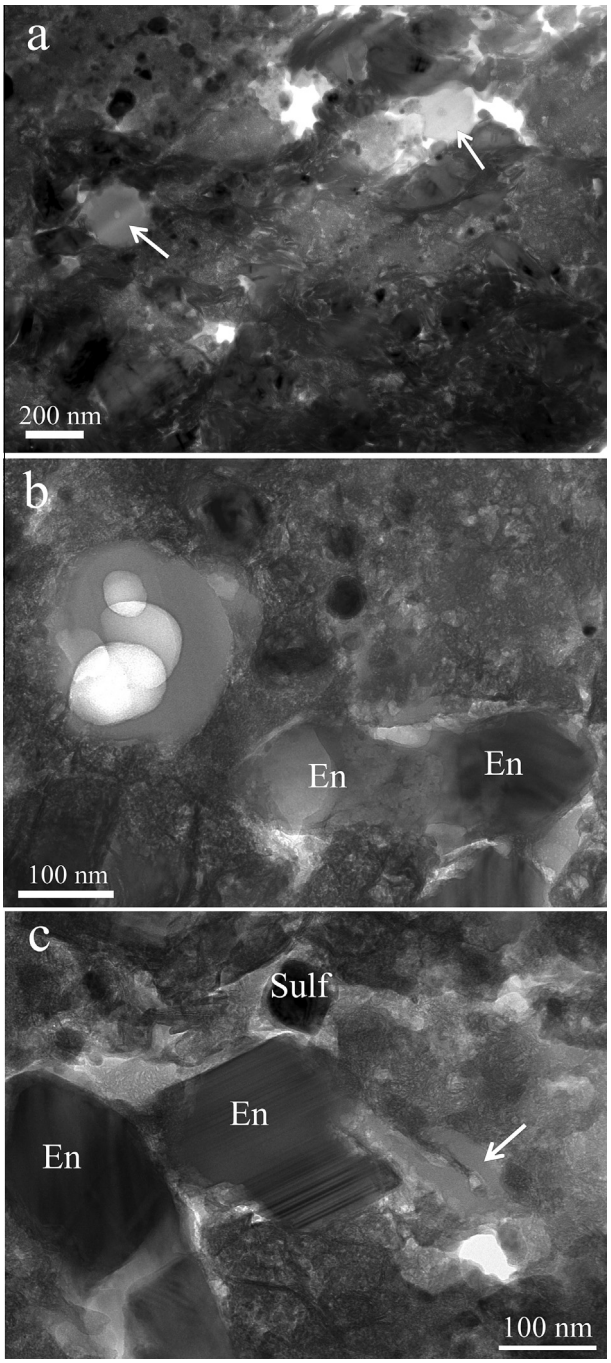

Fig. 12. Bright field TEM images showing the distribution of coarse-grained carbonaceous phases (a) rounded globules (arrowed) in a matrix mainly constituted of fibrous phyllosilicates. Amorphous areas are still present locally. (b) Hollow rounded-shaped globule in a finely fibrous matrix. En = Enstatite. (c) Curved lacey-shaped carbonaceous phase (arrowed), about 200 nm long and 30 nm thick. The surrounded matrix is amorphous, with a spongy aspect (light gray), to finely fibrous. En = enstatite; Sulf = Fe-sulfide.

Fe in the silicate groundmass of the matrix, together with leaching of Ca and S. The two CR chondrites QUE 99177 and MET00426, studied by Abreu and Brearley (2010), Keller and Messenger (2012) and Le Guillou and

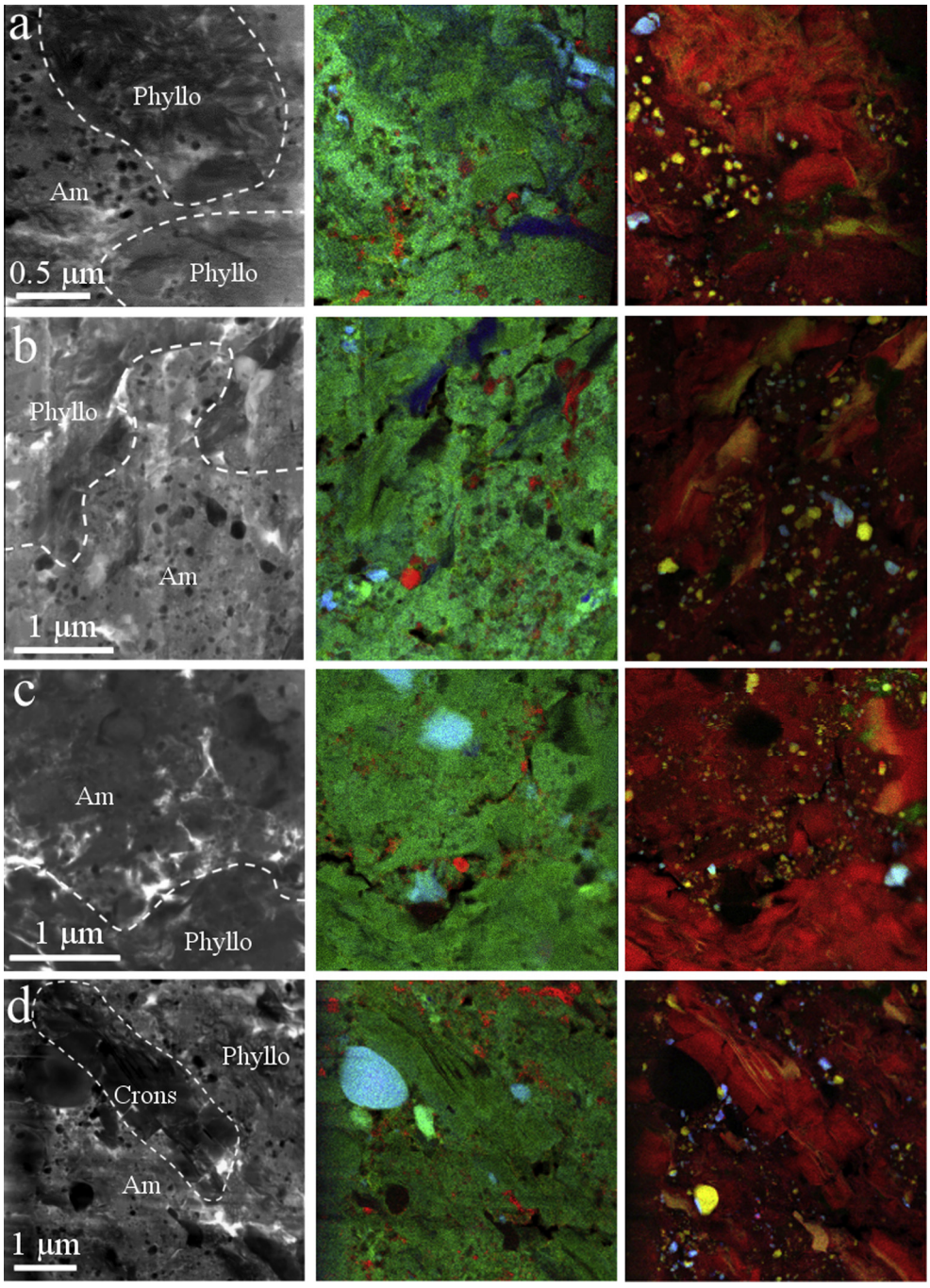

Fig. 13. Phase contrast images show strong microstructural heterogeneities in the altered matrix of Paris. Left: bright field images with 'Phyllo' for fibrous phyllosilicates, 'Am' for amorphous material and 'Crons' for platy cronstedtite. Middle: RGB images with C (red), Mg (blue) and Si (green) with amorphous or fibrous material in green, carbonaceous material in red, forsterite in light blue, enstatite in light green, and tochilinite in dark blue. Right: RGB images (Fe in red, Ni in blue and S in green), leading to silicates red- brown, Ni-poor sulfide grains yellow and Ni-rich sulfide (pentlandite) blue. (a and b) Strong heterogeneities: fibrous areas, and amorphous to finely fibrous material with sulfide inclusions. Tochilinite fibers (middle, dark blue) intimately admixed with fibrous phyllosilicates. More lacy carbon (b, upper part) in finely fibrous (red-brown) than in coarsely fibrous regions (light red). (c) Sharp interface between a fibrous region (bottom, deep red) and an amorphous region with nano-inclusions of Fe-sulfides (reddish brown upper part). (d) Large grain of cronstedtite (deep red) with oriented layers of tochilinite; large rounded grain of forsterite (middle, in blue) and smaller enstatite (in light green). (For interpretation of the references to colour in this figure legend, the reader is referred to the web version of this article.)

Brearley (2014), show an intermediate configuration, between the composition fields of Paris and Acfer 094. They are not shown on Fig. 14 because the methodology used to acquire the data was different (especially for the analyzed volumes, preventing the construction of composition fields for a direct comparison with Paris).

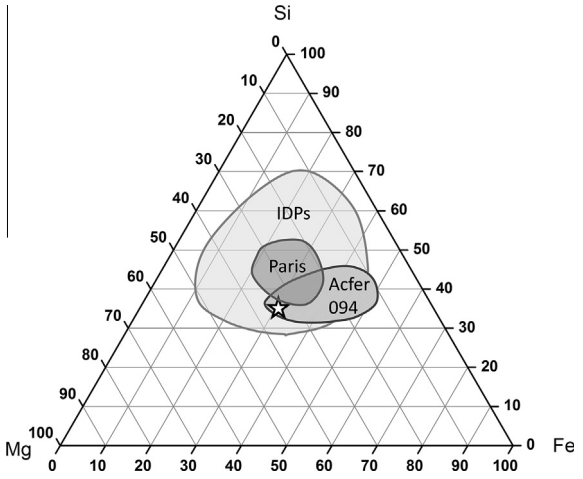

Fig. 14. Composition fields (at.%) of the GEMS-like material in Paris (this study), compared to those of IDPs (data from Keller and Messenger, 2011) and the amorphous silicates in Acfer 094 (data from Leroux et al., 2014). The star corresponds to the CI composition (Lodders, 2010). For these three composition fields, the analyzed volume of matter is comparable. The GEMS grains in IDPs have an average size close to 200 nm (Keller and Messenger, 2011). For Paris and Acfer 094, for each point of analysis that was used to construct the composition fields, the analyzed volume was 200 * 200 * 100 nm = 4.10^{-3} μm^3.

An essential feature of the fresh matrix of Paris is the degree of porosity, measured at 30%. In CM carbonaceous chondrites, the average is around 20% (e.g., Consolmagno et al., 2008). This value of 30% is lower than the average porosity measured in the carbonaceous asteroids (e.g., Britt et al., 2002) but these cases the high porosity is likely due to impact-generated fractures. In other matrices of primitive meteorites studied so far, porosities are well below that measured in the fresh areas of Paris. For instance, Abreu and Brearley (2010) measured a porosity of 7% in an FIB section of the matrix of QUE 99177, a CR chondrite classified 3.0. In more altered areas in which fibrous silicates are present, the porosity tends to disappear. This is certainly the consequence of fluid circulation and deposition of matter transported by these fluids into the initial porosity.

4.3. Early stage of aqueous alteration in a CM matrix

The heterogeneity of microstructures in the Paris matrix, from the least altered to more strongly altered regions, can be used to infer the sequence of alteration in a CM parent body. The sequence of progressive alteration, as deduced from our TEM observations, is illustrated schematically in Fig. 15. The corresponding chemical evolution is shown Fig. 16 on the Fe–Mg–Si ternary diagram. The predominant chemical evolution is an Fe-enrichment as the alteration microstructure develops. Fe was likely provided by a fluid phase circulating in the matrix.

As discussed above, the most primitive material consists of GEMS-like objects whose properties (presence of porosity and nanosulfide inclusions, persistence of the amorphous state and chemical composition close to CI) attest to limited aqueous alteration (Fig. 15a). The absence of metal nano-inclusions, the low concentration of Ca and the presence of pentlandite between the GEMS-like grains located within the intergranular space, shows that these regions could not fully escape alteration. Pentlandite crystallization certainly demonstrates that the first fluids that circulated in the intergranular space were rich in Fe, Ni and S, likely originating from the preferential consumption of metal and Fe-sulfide grains by fluids, as already proposed by Tomeoka and Buseck (1985), Zolensky et al. (1993), Hanowski and Brearley (2000) and Palmer and Lauretta (2011) among others. The solubilization of Fe species requires an oxidation by water and should generate significant H_2 (see Alexander et al., 2010 and references therein).

The second stage (Fig. 15b) involves the beginning of the formation of fine grained phyllosilicates, still poorly crystalline. They formed preferentially in the porosity that is progressively filled. This is likely due to fluid circulation and element deposition in the pore spaces. During this second stage, the amorphous silicates were not strongly affected, as attested by the main groundmass, which is amorphous and still contains numerous nano-sulfide inclusions. However, the assemblage amorphous material + fine grained phyllosilicates evolved in composition, becoming enriched in Fe while the ratio Mg/Si remained constant. This chemical evolution shows that the fluid that circulated was enriched in Fe, which is probably due to the easy breakdown of kamacite and Fe-sulfides during this early stage of aqueous alteration (e.g., Zolensky et al., 1993; Palmer and Lauretta, 2011). The local association with fine-grained phyllosilicates suggests that the amorphous phase interacted with water. This stage also likely involved the impregnation of the amorphous silicates by water, leading to a mottled contrast (or spongy aspect), locally with a poorly developed fibrous texture. Recently, the hydration of amorphous silicates in primitive chondrites has been documented in the context of early stage alteration (Keller and Messenger, 2012; Le Guillou and Brearley, 2014). For the Paris samples, the specific TEM/EDS method used by Le Guillou and Brearley (2014) to estimate the water content for the MET 00426 CR3.0 chondrite has not been applied. The water content in the amorphous silicate of Paris is thus unknown. As for MET 00426, this amorphous silicate is found frequently in contact with phyllosilicates and is thus probably hydrated.

Finally, the interaction of water with the amorphous silicates led to the formation of phyllosilicates, by replacement of the amorphous phase (crystallization in situ), as suggested by the close association between the two. Based on TEM studies, Lauretta et al. (2000), Chizmadia and Brearley (2008), Abreu and Brearley (2010) and Le Guillou and Brearley (2014) have reached the same conclusions. During this transformation, the nano-inclusions of Fe-sulfides were progressively dissolved but the relatively high S content in the fine-fibrous material suggests that S is likely included in fibrous tochilinite intricately intermixed with phyllosilicates. During this evolution (replacement of the amorphous silicates by fibrous material), the bulk

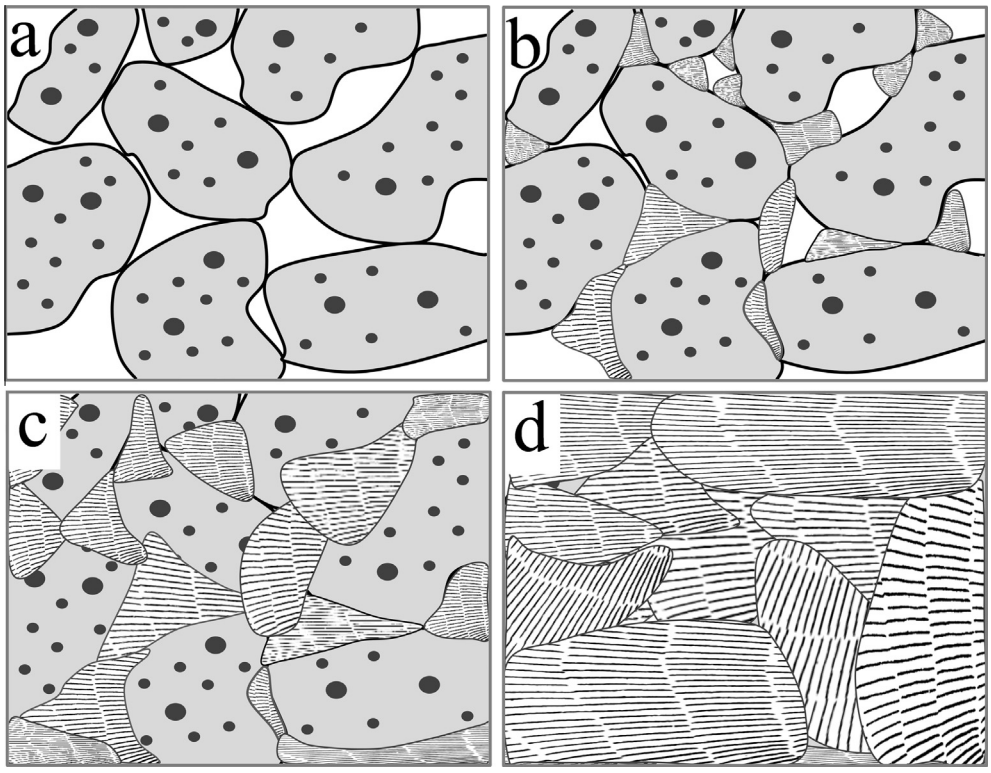

Fig. 15. Schematic representation of the evolution of the microstructure, as deduced from the TEM observations. The four panels correspond to different alteration degrees. (a) The starting material consists of amorphous units, containing nano-inclusions of Fe-sulfides, separated from one another by porosity. Corresponding Figs. 1 and 2. (b) Formation of fine grained silicates within the open spaces and at the edges of the amorphous units. Corresponding Fig. 4a and b. (c) Development of the fibrous texture with progressive replacement of the amorphous phase. The nano-inclusions of Fe-sulfides are transformed in the fibrous materials, probably as fibrous tochilinite intermixed with the fibrous silicates. Corresponding Fig. 4c and d. (d) The amorphous phase is fully consumed and the fibrous texture is becoming coarser. Corresponding Fig. 7.

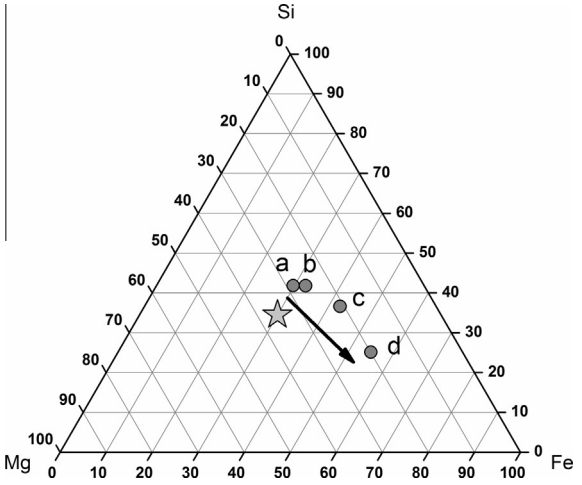

Fig. 16. Chemical evolution in the ternary diagram Fe–Mg–Si corresponding to the four stages schematized in Fig. 15. The compositions are averages based on the microstructure of the areas investigated. The composition fields of each sub-group are shown on Figs. 3a, 6b and 8.

concentration became enriched in Fe, but maintained an approximatively constant Mg/Si ratio. This shows that the fluid which accompanied the transformation is Fe-rich. Further evolution of the fibrous silicate led to coarsening and Fe-enrichment (see Fig. 15d). With progressive alteration, the compositions in the ternary diagram Fe–Mg–Si lie roughly along a line that extends from the CI composition (Fe30) toward the Fe-apex (Fe70). This line has an approximately constant Mg/Si ratio, showing that the enrichment with Fe affected the octahedral and tetrahedral sites in the silicate structure. This finding also shows that in the fibrous areas, the additional Fe is likely Fe^{+3}, compatible with an addition of Fe coming from an oxidized fluid.

The formation mechanism of platy cronstedtite is likely not related to the replacement features described above (leading to the formation of curved fine-grained serpentines). The well crystallized platy grains are present in all samples whatever the alteration degree, except the least altered. They are found in association with the different phases (amorphous, curved fine-grained to coarse grained). This suggests that the platy cronstedtite grains are formed in the early stage of alteration, likely within the initial porosity of the matrix from fluid precipitation. Cronstedtite as an early alteration phases has been proposed previously (e.g., McSween, 1979; Trigo-Rodriguez et al., 2006; Howard et al., 2009, 2011, 2015).

Hewins et al. (2014) showed that silicate minerals in chondrules are well preserved from alteration. Our TEM study shows that the small crystalline grains of Mg–silicates isolated in the matrix are also relatively well preserved. However, we detected some local replacement features, in particular for enstatite. The very small sized grains (typically below 100 nm) are not present in the altered regions (where the amorphous groundmass is converted into fine fibrous material). This observation indicates that they have been dissolved during alteration. In the altered regions, we show also that the Mg-rich silicates (forsterite and enstatite) have smooth and curves interfaces with the fibrous groundmass. Again it suggests a partial dissolution in the fibrous matrix, involving a preferential dissolution of apices to leave the final rounded surfaces. Lastly, it is remarkable that all the small crystalline anhydrous silicates in the matrix are all almost pure Mg–silicates. This means that the iron-containing silicates, if present before the aqueous alteration episode, are much less resistant to alteration. This hypothesis is consistent with previous observations that showed that ferroan olivine, isolated or from chondrules, is more extensively altered than coarse forsteritic olivine (e.g., Hanowski and Brearley, 2001; Rubin et al., 2007; Velbel et al., 2012, 2015). A number of studies showed that the dissolution kinetics of fayalitic olivine in water is several times faster than forsterite (e.g., Wogelius and Walther, 1992; Velbel, 1999; Rubin et al., 2007).

The Paris chondrite documents the early stage of alteration in a CM parent body. Later stages of alteration (not observed in Paris) would have proceeded by the dissolution of Mg-rich silicates (including those in chondrules) leading to fluids enriched in Mg, leading to the progressive evolution to Mg-rich serpentines as observed in the significantly altered CM chondrites. Indeed, the degree of alteration in CMs that are more altered than Paris is found to be correlated with the variation of matrix Mg and Fe abundances (McSween and Richardson, 1977; Tomeoka and Buseck, 1985; Zolensky et al., 1993; Browning et al., 1996; Rubin et al., 2007). Compared to the chemical evolution shown on Fig. 16, the chemical pathway for more altered CM chondrites is thus reversed and approaches values close to CI when chondrules are fully consumed.

5. CONCLUSION

A TEM examination of the matrix of Paris has been conducted. This matrix is found to be heterogeneous, even at the micro-scale. Some samples display alteration products similar to other altered CM chondrites, dominated by phyllosilicates. However, Paris also preserved very pristine material that has escaped significant aqueous alteration.

The least altered sample areas offer a good opportunity to decipher the characteristics of the accreted building blocks of the CM chondrites. The dominant microstructure consists of domains of amorphous silicates containing abundant nano-sulfide inclusions and separated by an abundant porosity. These microstructural properties share strong similarities with those of matrices of the other primitive carbonaceous chondrites studied so far (ALH A77307, Acfer 094, MET 00426 and QUE 99177), as well as with chondritic-porous IDPS, chondritic-porous micrometeorites and ultracarbonaceous micrometeorites. We conclude that GEMS-like grains could have been the building blocks of the Paris matrix material. Similarities with other primitive objects also suggest that GEMS grains are the main component of the dust of the solar nebula.

The altered areas share microstructural similarities with other CM matrices. They consist mainly of fibrous phyllosilicates, more or less developed, attesting to an aqueous alteration episode. The variability of the microstructure, also observed at the micron-scale, gives important insights about the evolution of the first stages of alteration of the fine-grained material, from the unaltered amorphous silicates to the fully transformed fibrous material. The first stage consists of a deposition of fine-fibrous material (phyllosilicate?) and coarse platy cronstedtite (with intercalated tochilinite) in the initial porosity space. The second stage involves the progressive replacement of the amorphous material by fine fibrous phyllosilicates. The final stage in Paris corresponds to coarsening, leading to well developed and well crystalline phyllosilicates. These stages correspond to silicate enrichment in Fe released by alteration of metal and sulfide. Subsequent reversal of this trend by Mg enrichment of phyllosilicate because of alteration of anhydrous Mg silicates, observed in normally altered CM chondrites, did not occur in our samples.

ACKNOWLEDGMENTS

We thank Ahmed Addad and Jean-François Dhenin for their constant assistance with the electron microscope instruments. We thank David Troadec for the FIB sections, prepared at IEMN, University of Lille. We thank Conel Alexander, Kieren Howard and Martin Lee for their thoughtful and comprehensive reviews that have significantly improved the manuscript, as well as the editorial handling by Eric Quirico. H.L. thanks the PNP (programme national de planétologie, CNRS-INSU) for the funding of the earliest investigations. The TEM work has been done at the electron microscope facility at the University of Lille with the support of the Chevreul Institute, the European FEDER and Région Nord-Pas-de-Calais. This work was partly supported by the French RENATECH network.

REFERENCES

Abreu N. M. and Brearley A. J. (2010) Early solar system processes recorded in the matrices of two highly pristine CR3 carbonaceous chondrites, MET00426 and QUE99177. *Geochim. Cosmochim. Acta* **74**, 1146–1171.

Alexander C. M. O'D., Newsome S. D., Fogel M. L., Nittler L. R., Busemann H. and Cody G. D. (2010) Deuterium enrichments in chondritic macromolecular material-implications for the origin and evolution of organics, water and asteroids. *Geochim. Cosmochim. Acta* **74**, 4417–4437.

Alexander C. M. O'D., Howard K. T., Bowden R. and Fogel M. L. (2013) The classification of CM and CR chondrites using bulk H, C and N abundances and isotopic compositions. *Geochim. Cosmochim. Acta* **123**, 244–260.

Barber D. J. (1981) Matrix phyllosilicates and associated minerals in C2M carbonaceous chondrites. *Geochim. Cosmochim. Acta* **45**, 945–970.

Barber D. J. (1985) Phyllosilicates and other layer-structured materials in stony meteorites. *Clay Miner.* **20**, 415–454.

Beck P., Quirico E., Montes-Hernandez G., Bonal L., Bollard J., Orthous-Daunay F.-R., Howard K. T., Schmitt B., Brissaud O., Deschamps F., Wunder B. and Guillot S. (2010) Hydrous mineralogy of CM and CI chondrites from infrared spectroscopy and their relationship with low albedo asteroids. *Geochim. Cosmochim. Acta* **74**, 4881–4892.

Beck P., Garenne A., Quirico E., Bonal L., Montes-Hernandez G., Moynier F. and Schmitt B. (2014) Transmission infrared spectra (2–25 μm) of carbonaceous chondrites (CI, CM, CV-CK, CR, C2 ungrouped): mineralogy, water, and asteroidal processes. *Icarus* **229**, 263–277.

Bland P. A., Jackson M. D., Coker R. F., Cohen B. A., Webber J. B. W., Lee M. R., Duffy C. M., Chater R. J., Ardakani M. G. and McPhail D. S. (2009) Why aqueous alteration in asteroids was isochemical: high porosity ≠ high permeability. *Earth Planet. Sci. Lett.* **287**, 559–568.

Bradley J. P., Brownlee D. E. and Veblen D. R. (1983) Pyroxene whiskers and platelets in interplanetary dust – evidence of vapour phase growth. *Nature* **301**, 473–477.

Bradley J. P. (1994) Nanometer-scale mineralogy and petrography of fine-grained aggregates in anhydrous interplanetary dust particles. *Geochim. Cosmochim. Acta* **58**, 2123–2134.

Brearley A. J. (1993) Matrix and fine-grained rims in the unequilibrated CO3 chondrite, ALHA77307: origins and evidence for diverse, primitive nebular dust components. *Geochim. Cosmochim. Acta* **57**, 1521–1550.

Brearley A. J. (2006) The action of water. In *Meteorites and the Early Solar System II* (eds. D. S. Lauretta and , Jr.H. Y. McSween). Univ. Arizona University Press, pp. 587–624.

Britt D. T., Yeomans D. K., Housen K. R. and Consolmagno G. J. (2002) Asteroid density, porosity and structure. In *Asteroids III* (eds. W. Bottke, A. Cellino, P. Paolicchi and R. Binzel). University of Arizona Press, Tucson, pp. 485–500.

Browning L. B., McSween, Jr., H. Y. and Zolensky M. E. (1996) Correlated alteration effects in CM carbonaceous chondrites. *Geochim. Cosmochim. Acta* **60**, 2621–2633.

Chizmadia L. J., Nuth III J. A. and Rietmeijer F. J. M. (2006) Experimental aqueous alteration of amorphous silicate smokes. *Lunar Planet. Sci. XXXVII*. Lunar Planet. Inst., Houston. #2187 (abstr.).

Chizmadia L. J. and Brearley A. J. (2008) Mineralogy, aqueous alteration, and primitive textural characteristics of fine-grained rims in the Y-791198 CM2 carbonaceous chondrite: TEM observations and comparison to ALHA81002. *Geochim. Cosmochim. Acta* **72**, 602–625.

Consolmagno G. J., Britt D. T. and Macke R. J. (2008) The significance of meteorite density and porosity. *Chem. Erde* **68**, 1–29.

De Gregorio B. T., Stroud R. M., Nittler L. R., Alexander C. M. O'D., Kilcoyne A. L. D. and Zega T. J. (2010) Isotopic anomalies in organic nanoglobules from comet 81P/Wild 2: comparison to Murchison nanoglobules and isotopic anomalies induced in terrestrial organics by electron irradiation. *Geochim. Cosmochim. Acta* **74**, 4454–4470.

De Gregorio B. T., Stroud R. M., Nittler L. R., Alexander C. M. O'D., Bassim N. D., Cody G. D., Kilcoyne A. L. D., Sandford S. A., Milam S. N., Nuevo M. and Zega T. J. (2013) Isotopic and chemical variation of organic nanoglobules in primitive meteorites. *Meteorit. Planet. Sci.* **48**, 904–928.

Dobrică E., Engrand C., Leroux H., Rouzaud J. N. and Duprat J. (2012) Transmission electron microscopy of CONCORDIA ultracarbonaceous Antarctic micrometeorites (UCAMMs): mineralogical properties. *Geochim. Cosmochim. Acta* **76**, 68–82.

Garvie L. A. J. and Buseck P. R. (2004) Nanosized carbon-rich grains in carbonaceous chondrite meteorites. *Earth Planet. Sci. Lett.* **224**, 431–439.

Greshake A. (1997) The primitive matrix components of the unique carbonaceous chondrite Acfer 094: a TEM study. *Geochim. Cosmochim. Acta* **61**, 437–452.

Grossman J. N. and Brearley A. J. (2005) The onset of metamorphism in ordinary and carbonaceous chondrites. *Meteorit. Planet. Sci.* **40**, 87–122.

Hanowski N. P. and Brearley A. J. (2000) Iron-rich aureoles in the CM carbonaceous chondrites Murray, Murchison, and Allan Hills 81002: evidence for in situ aqueous alteration. *Meteorit. Planet. Sci.* **35**, 1291–1308.

Hanowski N. P. and Brearley A. J. (2001) Aqueous alteration of chondrules in the CM carbonaceous chondrite, Allan Hills 81002: implications for parent body alteration. *Geochim. Cosmochim. Acta* **65**, 495–518.

Hewins R. H., Bourot-Denise M., Zanda B., Leroux H., Barrat J. A., Humayun M., Göpel C., Greenwood R. C., Franchi I. A., Pont S., Lorand J. P., Cournède C., Gattacceca J., Rochette P., Kuga M., Marrocchi Y. and Marty B. (2014) The Paris meteorite, the least altered CM chondrite so far. *Geochim. Cosmochim. Acta* **124**, 190–222.

Hybler J., Petříček V., Ďurovič S. and Smrčok Ľ. (2000) Refinement of the crystal structure of cronstedtite-1T. *Clays Clay Miner.* **48**, 331–338.

Howard K. T., Benedix G. K., Bland P. A. and Cressey G. (2009) Modal mineralogy of CM2 chondrites by X-ray diffraction (PSD-XRD). Part 1: total phyllosilicate abundance and the degree of aqueous alteration. *Geochim. Cosmochim. Acta* **73**, 4576–4589.

Howard K. T., Benedix G. K., Bland P. A. and Cressey G. (2011) Modal mineralogy of CM chondrites by X-ray diffraction (PSD-XRD): Part 2. Degree, nature and settings of aqueous alteration. *Geochim. Cosmochim. Acta* **75**, 2735–2751.

Howard K. T., Alexander C. M. O'D., Schrader D. L. and Dyl K. A. (2015) Classification of hydrous meteorites (CR, CM and C2 ungrouped) by phyllosilicate fraction: PSD-XRD modal mineralogy and planetesimal environments. *Geochim. Cosmochim. Acta* **149**, 206–222.

Janney D. E., Cowley J. M. and Buseck P. R. (2000) Transmission electron microscopy of synthetic 2- and 6-line ferrihydrite. *Clays Clay Miner.* **48**, 111–119.

Keller L. P. and Messenger S. (2011) On the origins of GEMS grains. *Geochim. Cosmochim. Acta* **75**, 5336–5365.

Keller L. P. and Messenger S. (2012) Formation and processing of amorphous silicates in primitive carbonaceous chondrites and cometary dust. *Lunar Planet. Sci. XLIII*. Lunar Planet. Inst., Houston. #1880 (abstr.).

Lauretta D. S., Hua X. and Buseck P. R. (2000) Mineralogy of fine-grained rims in the ALHA81002 CM chondrite. *Geochim. Cosmochim. Acta* **64**, 3263–3273.

Lee M. R., Lindgren P. and Sofe M. R. (2014) Aragonite, breunnerite, calcite and dolomite in the CM carbonaceous chondrites: high fidelity recorders of progressive parent body aqueous alteration. *Geochim. Cosmochim. Acta* **144**, 126–156.

Le Guillou C. and Brearley A. J. (2014) Relationships between organics, water and early stages of aqueous alteration in the pristine CR3.0 chondrite MET 00426. *Geochim. Cosmochim. Acta* **131**, 344–367.

Leroux H., Cuvillier P., Zanda B. and Hewins R. H. (2014) Submicrometer composition fields of Acfer 094 and Paris matrices. *Lunar Planet. Sci. XLV*. Lunar Planet. Inst., Houston. #1706 (abstr.).

Lindgren P. and Lee M. R. (2015) Tracking the earliest stages of aqueous alteration in the mildly altered CM chondrite EET

96029. *Lunar Planet. Sci. XLVI.* Lunar Planet. Inst., Houston. #1760 (abstr.).

Lodders K. (2010) Solar system abundances of the elements. In *Principles and Perspectives in Cosmochemistry* (eds. A. Goswami and B. E. Reddy). Astrophysics and Space Science Proceedings, Springer-Verlag, Berlin, pp. 379–417.

Matrajt G., Messenger S., Brownlee D. and Joswiak D. (2012) Diverse forms of primordial organic matter identified in interplanetary dust particles. *Meteorit. Planet. Sci.* **47**, 525–549.

Marrocchi Y., Gounelle M., Blanchard I., Caste F. and Kearsley A. T. (2014) The Paris CM chondrite: secondary minerals and asteroidal processing. *Meteorit. Planet Sci.* **49**, 1232–1249.

McSween, Jr., H. Y. (1979) Alteration in CM carbonaceous chondrites inferred from modal and chemical variations in matrix. *Geochim. Cosmochim. Acta* **43**, 1761–1770.

McSween, Jr., H. Y. (1987) Aqueous alteration in carbonaceous chondrites: mass balance constraints on matrix mineralogy. *Geochim. Cosmochim. Acta* **51**, 2469–2477.

McSween, Jr., H. Y. and Richardson S. M. (1977) The composition of carbonaceous matrix. *Geochim. Cosmochim. Acta* **41**, 1145–1161.

Nakamura-Messenger K., Messenger S., Keller L. P., Clemett S. J. and Zolensky M. E. (2006) Organic globules in the Tagish Lake meteorite: remnants of the protosolar disk. *Science* **314**, 1439–1442.

Nakamura-Messenger K., Clemett S. J., Messenger S. and Keller L. P. (2011) Experimental aqueous alteration of cometary dust. *Meteorit. Planet. Sci.* **46**, 843–856.

Noguchi T., Ohashi N., Tsujimoto S., Mitsunari T., Bradley J. P., Nakamura T., Toh S., Stephan T., Iwata N. and Imae N. (2015) Cometary dust in Antarctic ice and snow: past and present chondritic porous micrometeorites preserved on the Earth's surface. *Earth Planet. Sci. Lett.* **410**, 1–11.

Palmer E. E. and Lauretta D. S. (2011) Aqueous alteration of kamacite in CM chondrites. *Meteorit. Planet. Sci.* **46**, 1587–1607.

Rietmeijer F. J. M., Nuth, III, J. A. and Nelson R. N. (2004) Laboratory hydration of condensed magnesiosilica smokes with implications for hydrated silicates in IDPs and comets. *Meteorit. Planet. Sci.* **39**, 723–746.

Rubin A. E., Trigo-Rodriguez J. M., Huber H. and Wasson J. T. (2007) Progressive alteration of CM carbonaceous chondrites. *Geochim. Cosmochim. Acta* **71**, 2361–2382.

Tomeoka K. and Buseck P. R. (1985) Indicators of aqueous alteration in CM carbonaceous chondrites: microtextures of a layered mineral containing Fe, S, O and Ni. *Geochim. Cosmochim. Acta* **49**, 2149–2163.

Tomeoka K., McSween, Jr., H. Y. and Buseck P. R. (1989) Mineralogical alteration of CM carbonaceous chondrites: a review. *Antarct. Meteorit. Res.* **2**, 221–234.

Trigo-Rodriguez J. M., Rubin A. E. and Wasson J. T. (2006) Non-nebular origin of dark mantles around chondrules and inclusions in CM chondrites. *Geochim. Cosmochim. Acta* **70**, 1271–1290.

van Cappellen E. (1990) The parameterless correction method in X-ray microanalysis. *Microsc. Microanal. Microstruct.* **1**, 1–22.

Van Cappellen E. and Doukhan J. C. (1994) Quantitative transmission X-ray microanalysis of ionic compounds. *Ultramicroscopy* **53**, 343–349.

Velbel M. A. (1999) Bond strength and the relative weathering rates of simple orthosilicates. *Am. J. Sci.* **299**, 679–696.

Velbel M. A. and Palmer E. E. (2011) Fine-grained serpentine in CM2 carbonaceous chondrites and its implications for the extent of aqueous alteration on the parent body: a review. *Clays Clay Miner.* **59**, 416–432.

Velbel M. A., Tonui E. K. and Zolensky M. E. (2012) Replacement of olivine by serpentine in the carbonaceous chondrite Nogoya (CM2). *Geochim. Cosmochim. Acta* **87**, 117–135.

Velbel M. A., Tonui E. K. and Zolensky M. E. (2015) Replacement of olivine by serpentine in the Queen Alexandra Range 93005 carbonaceous chondrite (CM2): reactant–product compositional relations, and isovolumetric constraints on reaction stoichiometry and elemental mobility during aqueous alteration. *Geochim. Cosmochim. Acta* **148**, 402–425.

Wogelius R. A. and Walther J. V. (1992) Olivine dissolution kinetics at near-surface conditions. *Chem. Geol.* **97**, 101–112.

Zega T. J. and Buseck P. R. (2003) Fine-grained-rim mineralogy of the Cold Bokkeveld CM chondrite. *Geochim. Cosmochim. Acta* **67**, 1711–1721.

Zolensky M. E., Barrett R. and Browning L. (1993) Mineralogy and composition of matrix and chondrule rims in carbonaceous chondrites. *Geochim. Cosmochim. Acta* **57**, 3123–3148.

Zolensky M. E., Mittlefehldt D. W., Lipshutz M. E., Wang M., Clayton R. N., Mayeda T. K., Grady M. M., Pillinger C. T. and Barber D. (1997) CM chondrites exhibit the complete petrologic range from type 2 to 1. *Geochim. Cosmochim. Acta* **61**, 5099–5115.

Associate editor: Eric Quirico